Surgical Procedures

All experimental animals used in these studies were maintained and treated according to the guidelines for the care and use of laboratory animals of the Tokyo Medical and Dental University. After anesthesia by intraperitoneal administration of 7% trichloroacetaldehyde monohydrate solution (0.5 mL per 100 g of body weight) and aseptic preparation, HAp/Col implants were transplanted into bone defects created in the distal ends of the femurs and into pouches in the back muscles of male rats (F344, age 11 weeks, weight 240–250 g). The distal end of the femur shaft was exposed by lateral approach and a 3-mm diameter hole was bored using an electric drill with continuous saline irrigation. The drill hole was then rinsed with saline, and the implant was placed in the hole. At 2, 4, and 8 weeks post-transplantation, the rats were euthanized and the femurs and composites transplanted into the back muscles were excised.

Quantification of Porous HAp/Col in Back Muscle

Porous HAp/Col implants removed from the dorsal muscle were scanned using a micro-CT scanner (ScanXmate-E090; Comscantecno, Japan) before fixation to exclude the effects of fixation on sample volume. Three-dimensional image data were then reconstructed, and the volume of the porous implant was calculated using the three-dimensional bone analysis software TRI/3D-BON (Ratoc System Engineering, Japan).

Histological Analysis

After micro-CT analysis, samples were fixed in 4% paraformaldehyde, decalcified in 20% ethylenediaminetetraacetic acid (EDTA), dehydrated using a graded alcohol series, and embedded in paraffin wax. Sections of 5-μm thickness were cut and stained with hematoxylin and eosin (HE) or tartrate-resistant acid phosphatase stain (TRAP).

Statistical Analysis

Overall differences among groups in the mechanical test were determined by two-factor repeated measures analysis of variance (ANOVA), and those in the other experiments were determined by two-factor ANOVA, and differences between individual groups were estimated using the Tukey-Kramer multiple comparison test. Differences were considered statistically significant when the p value was <0.05.

RESULTS

Compressive Mechanical Test

Swelling of the samples after rehydration was not detected by macroscopic observation. All tested samples behaved elastically, and recovery rates after the fourth compression were greater than 92% in all groups, although there was a slight irradiation dose-dependent decrease in recovery rate (Table I). Compared to the nonirradiated control, the compressive elastic modulus of all irradiated groups was markedly decreased at strains of both 10 and 20%, with the lowest modulus observed in the 50-kGy group [Figure 1(A)]. SEM images of porous HAp/Col specimens after mechanical testing demonstrated that although slight compressive deformation of the porous structures remained, there was no apparent disruption of the materials in any group, including those treated with 50-kGy irradiation [Figure 1(B)].

TABLE I. Recovery Rates of Compression Test

Control	16 kGy	25 kGy	35 kGy	50 kGy
94.3%	93.4%	93.5%	93.1%	92.8%

In Vitro Bioresorbability

Figure 2 shows the remaining weight of the HAp/Col composite after enzymatic digestion by collagenase. As the irradiation dose increased, the remaining weight decreased. The reduction ratios of the remaining porous HAp/Col in the 35- and 50-kGy groups were significantly higher than those of the other groups.

Quantification of Porous HAp/Col in Back Muscle

Figure 3 shows the volume of residual porous HAp/Col extracted from the back muscle. Control implants were scarcely absorbed until 8 weeks after transplantation. In contrast, all irradiated implants showed dose-dependent decrease in volume, with the 35- and 50-kGy irradiation-treated specimens exhibiting drastic volume decreases 2 weeks postoperatively. The average volume of the 50-kGy group was increased slightly at 4 and 8 weeks, where this may have been due to dispersion of the fragmented implant following tissue invasion.

Histological Analysis

Porous HAp/Col at the Extraskeletal Site. Fragmentation of porous HAp/Col implants and multinucleated macrophage attachment were observed in all irradiated groups at 2 weeks post-transplantation. The 50-kGy-treated implants were the most severely fragmented and reduced, with a large number of multinucleated macrophages attaching to the fragments. In the control group, despite the presence of macrophages, the porous structure of the extracted implants was maintained (Figure 4).

At 4 weeks after implantation, although the extracted implants in the 16-, 25-, and 35-kGy groups were almost completely fragmented and the original porous structures could not be recognized, the volume of the remnants of the 35- and the 50-kGy implants was still lower. Partial fragmentation of the control implant was also observed at 4 weeks postoperatively. At 8 weeks, absorption of the 25-

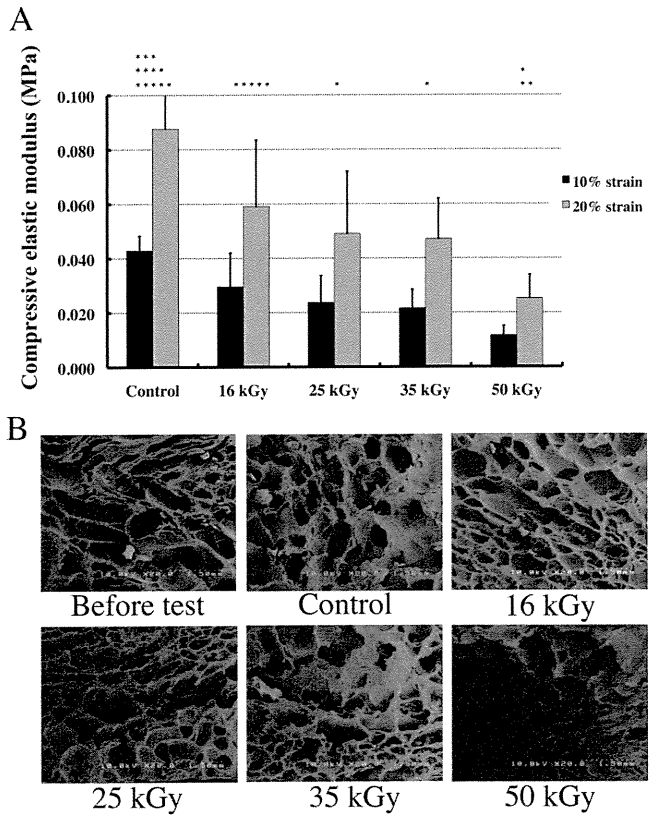

Figure 1. (A) Elastic moduli of porous HAp/Col after gamma-ray irradiation at 10 and 20% strain ($N = 5$). *$p < 0.05$ versus control, **$p < 0.05$ versus 16 kGy, ***$p < 0.05$ versus 25 kGy, ****$p < 0.05$ versus 35 kGy, *****$p < 0.05$ versus 50 kGy. (B) SEM images of the porous structure of HAp/Col before and after compression testing.

kGy implant was advanced when compared with the 16-kGy and control groups. Some control implants even maintained their original porous structure at 8 weeks.

Porous HAp/Col at the Skeletal Site. At 2 weeks after implantation, absorption of the irradiated implants was

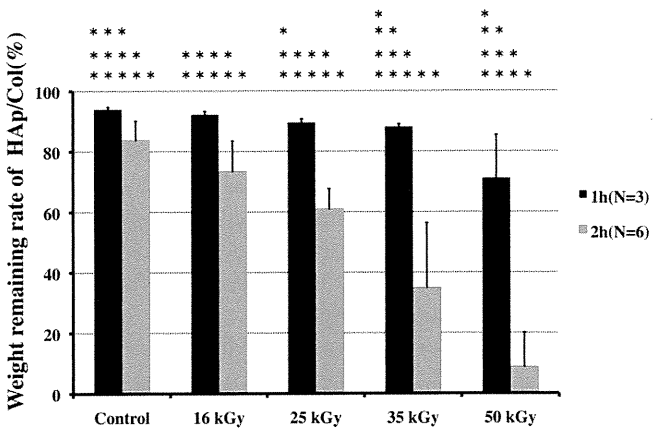

Figure 2. Weight of porous HAp/Col remaining after collagenase digestion. Incubation time of 1 ($N = 3$) or 2 h ($N = 6$). *$p < 0.05$ versus control, **$p < 0.05$ versus 16 kGy, ***$p < 0.05$ versus 25 kGy, ****$p < 0.05$ versus 35 kGy, *****$p < 0.05$ versus 50 kGy.

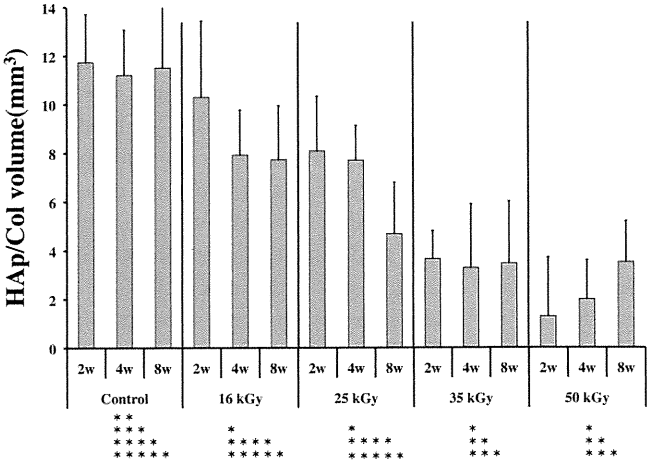

Figure 3. Residual volume of porous HAp/Col in back muscle quantified by micro-CT analysis. *$p < 0.05$ versus control, **$p < 0.05$ versus 16 kGy, ***$p < 0.05$ versus 25 kGy, ****$p < 0.05$ versus 35 kGy, *****$p < 0.05$ versus 50 kGy.

dose-dependent, with bioabsorption, fragmentation, and soft tissue invasion from the extraskeletal site observed for 50-kGy implants. Bone formation in the marrow cavity also showed irradiation dose-dependent increases (Figure 5).

At 4 weeks postoperatively, the bone defects of each group were almost completely closed, with no significant differences in the amount of residual implant or bone tissue in the marrow cavity. At 8 weeks, normal bone marrow cavities were restored; implants and surplus bone in the cavities were almost completely absorbed, and small remnants of the implants surrounded by the bone tissue were observed in all groups.

In 2-week implants, TRAP-positive multinucleated cells were attached to both the cavity and extraskeletal sides, and the number of TRAP-positive cells increased as the irradiation dose increased (Figure 6).

The 4-week implants also exhibited a large number of TRAP-positive cells in every group. The cells were mainly attached to newly formed bone in the 50-kGy gamma-irradiated implants, whereas in the control group, cells mainly adhered to the implant remnant. The number of TRAP-positive cells was markedly decreased at 8 weeks when compared with 2 and 4 weeks postimplantation.

DISCUSSION

In this study, gamma-ray irradiation resulted in dose-dependent reduction of elastic modulus and resistance to biological digestion for porous HAp/Col, although bone conductivity at skeletal implantation sites was not impaired.

Gamma-ray irradiation from Cobalt 60 sources is a popular sterilization method for medical devices, including implant materials. However, gamma-ray irradiation has also been reported to degrade collagen by splitting the peptide chains, thus adversely affecting the mechanical and biological properties of collagen-containing materials.[13,17] Porous

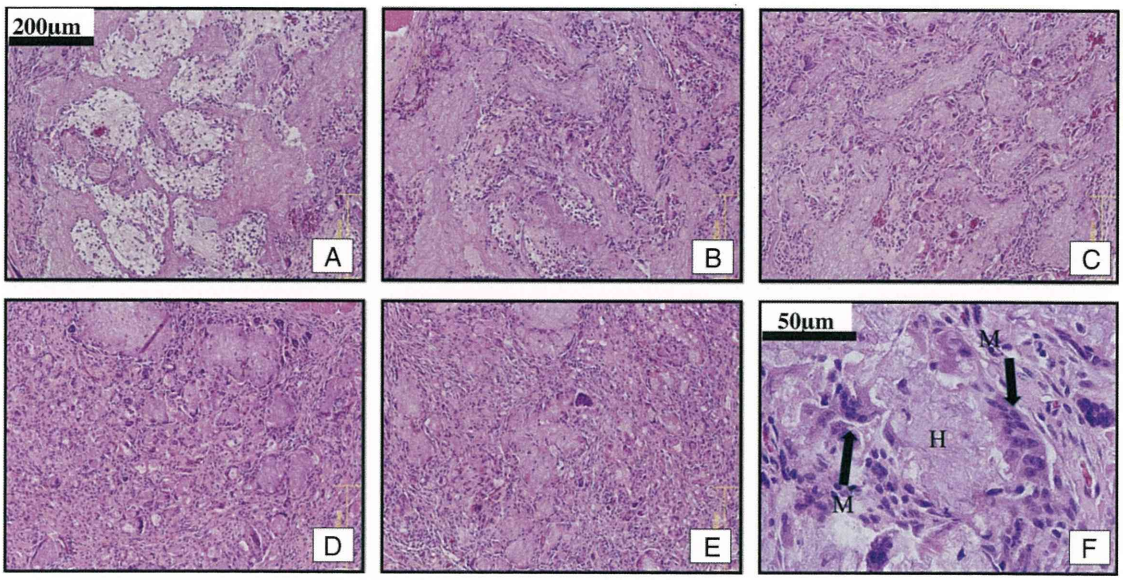

Figure 4. Sections of the HAp/Col implant harvested from back muscle at 2 weeks after implantation (HE staining). (A) Control group (70% ethanol), (B) 16-kGy-irradiated group, (C) 25-kGy-irradiated group, (D) 35-kGy-irradiated group, (E) 50-kGy-irradiated group, (F) high-magnification views of 25-kGy-irradiated group. H, HAp/Col. M, multinucleated macrophage. Implant fragmentation in the 35- and 50-kGy groups was severe. [Color figure can be viewed in the online issue, which is available at www.interscience.wiley.com.]

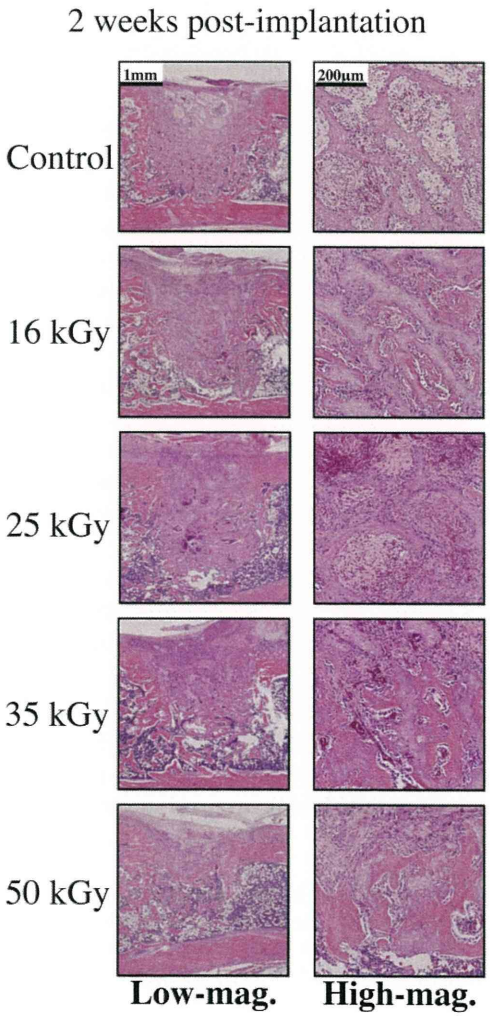

HAp/Col is a bioabsorbable bone substitute with high osteoconductivity and unique mechanical properties including elasticity; these properties permit facile handling during surgery.[9,18,19] Thus, the fragmentation of collagen fibers in HAp/Col by gamma-ray irradiation may significantly affect the ease of use of porous HAp/Col implants.

Porous HAp/Col is elastic and sponge-like and does not have weight-bearing mechanical strength. As a result, its mechanical properties do not contribute directly to its clinical usefulness and, for orthopedic applications, fixation devices must also be used at weight-bearing sites. However, the elasticity of HAp/Col is important for ease of handling and implantation, and therefore, we evaluated the effects of gamma-ray irradiation on elasticity. The elastic moduli of all HAp/Col implants showed irradiation dose-dependent decrease, with the most noticeable decrease observed for the 50-kGy group. Additionally, the 50-kGy-irradiated implants were noticeably fragile during *in vivo* transplantation experiments, although SEM images and the recovery rate after uniaxial compression did not reveal much degradation.

Bone prosthetic materials are commonly used to fill bone defects and accelerate natural bone ingrowth. Ideally, these materials should be absorbed and completely replaced

Figure 5. Coronal sections of femurs crossing the center of the implant 2 weeks postoperatively (HE staining). Left column shows lower magnification (×1.25), right column shows higher magnification (×10). [Color figure can be viewed in the online issue, which is available at www.interscience.wiley.com.]

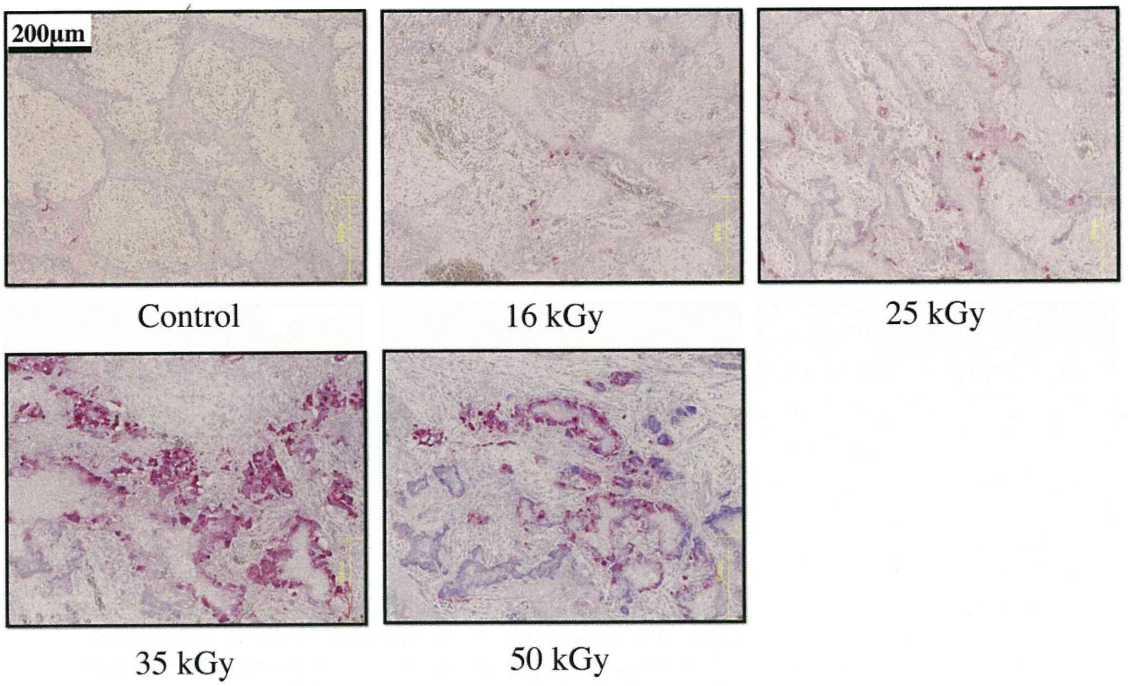

Figure 6. TRAP staining of femur sections 2 weeks postoperatively. The number of TRAP-positive cells was irradiation dose-dependent. [Color figure can be viewed in the online issue, which is available at www.interscience.wiley.com.]

by natural bone in the long term. However, in the clinic, bone defects are not always surrounded by cortical bone or periosteum, and healing may be disrupted by soft tissue invasion of the defect.[20] Bone substitutes implanted in bone defects promote healing by accelerating bone ingrowth due to osteoconductivity and prevention of soft tissue invasion.[21,22] Hence, bone substitutes should resist bioabsorption by macrophages with subsequent soft tissue invasion. Therefore, the effects of gamma-ray irradiation on the bioabsorbability of porous HAp/Col were tested using *in vitro* enzymatic digestion test and *in vivo* implantation models.

In vitro tests were performed using collagenase, which is responsible for collagen degradation *in vivo*.[16] *In vitro* digestion of the HAp/Col implant by collagenase was irradiation dose-dependent, with particularly notable degradation after gamma-ray irradiation at 35 or 50 kGy.

In muscular tissue, the porous HAp/Col nonirradiated implant maintained its volume and porous structure until 8 weeks after implantation, whereas in skeletal implantation sites, implants were almost completely absorbed and replaced by bone tissue. Control implants resisted bioabsorption from the extraskeletal site and soft tissue invasion. Intramuscular absorption of irradiated HAp/Col progressed faster than that of the control, especially for 35-and 50-kGy implants, whose volume decreased markedly at early time points. Absorption of the irradiated implants in the marrow cavities also progressed faster than that of the control, although this absorption was followed by the ingrowth of new bone. Notably, implant absorption and bone ingrowth were synchronized; thus, bone ingrowth of the 50-kGy group was most vigorous at early time points after transplantation. These findings indicate that osteoclast–osteoblast coupling mechanisms might be involved in the osteoconductivity of porous HAp/Col. Although all bone defects treated with irradiated implants eventually healed in the *in vivo* model, concavity and soft tissue invasion were observed on the extraskeletal side of 50-kGy implants due to macrophage adhesion. Thus, if the bone defects had been larger and a porous HAp/Col implant sterilized with 50 kGy or more gamma-ray irradiation had been transplanted, the implant may have been absorbed and the defect may not have healed completely.

In this study, porous HAp/Col was treated with gamma-ray irradiation at 16, 25, 35, and 50 kGy. Irradiation of porous HAp/Col at 16 kGy is the minimum dose for which we could validate sterility (ISO11137-2006, data not shown). Gamma-ray irradiation of porous HAp/Col has few beneficial effects and should thus be applied sparingly. Our results suggest that the proper gamma-ray irradiation dose for sterilization of porous HAp/Col is 16 or 25 kGy.

Porous HAp/Col was jointly developed by the Tokyo Medical and Dental University, the HOYA Corporation, and the National Institute for Materials Science (NIMS). The authors thank Dr. Masanori Kikuchi at NIMS for excellent technical support and advice.

REFERENCES

1. Perry CR. Bone repair techniques, bone graft, and bone graft substitutes. Clin Orthop Relat Res 1999;360:71–86.
2. Giannoudis PV, Dinopoulos H, Tsiridis E. Bone substitutes: An update. Injury 2005;36 (Suppl 3): S20–S27.
3. Finkemeier CG. Bone-grafting and bone-graft substitutes. J Bone Joint Surg Am 2002;84:454–464.
4. Reynolds MA, Aichelmann-Reidy ME, Branch-Mays GL, Gunsolley JC. The efficacy of bone replacement grafts in the treatment of periodontal osseous defects. A systematic review. Ann Periodontol 2003;8:227–265;Review.
5. Kikuchi M, Itoh S, Ichinose S, Shinomiya K, Tanaka J. Self-organization mechanism in a bone-like hydroxyapatite/collagen nanocomposite synthesized in vitro and its biological reaction in vivo. Biomaterials 2001;22:1705–1711.
6. Itoh S, Kikuchi M, Takakuda K, Koyama Y, Matsumoto H, Ichinose S, Tanaka J, Kawauchi T, Shinomiya K. The biocompatibility and osteoconductive activity of a novel hydroxyapatite/collagen composite biomaterial, and its function as a carrier of rhBMP-2. J Biomed Mater Res 2001;54:445–453.
7. Itoh S, Kikuchi M, Koyama Y, Takakuda K, Shinomiya K, Tanaka J. Development of an artificial vertebral body using a novel biomaterial, hydroxyapatite/collagen composite. Biomaterials 2002;23:3919–3926.
8. Sotome S, Uemura T, Kikuchi M, Chen J, Itoh S, Tanaka J, Tateishi T, Shinomiya K. Synthesis and in vivo evaluation of a novel hydroxyapatite/collagen–alginate as a bone filler and a drug delivery carrier of bone morphogenetic protein. Mater Sci Eng C 2004;24:341–347.
9. Sotome S, Orii H, Kikuchi M, Ikoma T, Ishida A, Tanaka J, Shinomiya K. In vivo evaluation of porous hydroxyapatite/collagen composite as a carrier of OP-1 in a rabbit PLF model. Key Eng Mater 2005;309–311:977–980.
10. Sotome S, Uemura T, Kikuchi M, Itoh S, Takakuda K, Tanaka J, Tateishi T, Shinomiya K. In vitro evaluation of highly absorptive ceramics materials needs consideration of calcium and magnesium ions adsorbed to the materials. Key Eng Mater 2002;218–220:153–156.
11. Xiaodu W, Ruud AB, Johan MT, Mauli A. The role of collagen in determining bone mechanical properties. J Orthop Res 2001:19:1021–1026.
12. Draenert GF, Delius M. The mechanically stable steam sterilization of bone grafts. Biomaterials 2007;28:1531–1538.
13. Nguyen H, Morgan DA, Forwood MR. Sterilization of allograft bone: Effects of gamma irradiation on allograft biology and biomechanics. Cell Tissue Bank 2007;8:93–105.
14. Noah EM, Chen J, Jiao X, Heschel I, Pallua N. Impact of sterilization on the porous design and cell behavior in collagen sponges prepared for tissue engineering. Biomaterials 2002;23:2855–2861.
15. Jinno T, Miric A, Feighan J, Kirk SK Davy DT, Stevenson S. The effects of processing and low dose irradiation on cortical bone grafts. Clin Orthop Relat Res 2000;375:275–285.
16. Yunoki S, Marukawa E, Ikoma T, Sotome S, Fan H, Zhang X, Shinomiya K, Tanaka J. Effect of collagen fibril formation on bioresorbability of hydroxyapatite/collagen composites. J Mater Sci Mater Med 2007;18:2179–2183.
17. Yunoki S, Ikoma T, Monkawa A, Ohta K, Tanaka J, Sotome S, Shinomiya K. Influence of gamma irradiation on the mechanical strength and in vitro biodegradation of porous hydroxyapatite/collagen composite. J Am Ceram Soc 2006:89: 297–299.
18. Yunoki S, Ikoma T, Monkawa A, Marukawa E, Sotome S, Shinomiya K, Tanaka J. Three-dimensional porous hydroxyapatite/collagen composite with rubber-like elasticity. J Biomater Sci Polym Ed 2007;18:393–409.
19. Yunoki S, Ikoma T, Tsuchiya A, Monkawa A, Ohta K, Sotome S, Shinomiya K, Tanaka J. Fabrication and mechanical and tissue ingrowth properties of unidirectionally porous hydroxyapatite/collagen composite. J Biomed Mater Res B Appl Biomater 2007;80:166–173.
20. Schmitz JP, Schwartz Z, Hollinger JO, Boyan BD. Characterization of rat calvarial nonunion defects. Acta Anat 1990;138: 185–192.
21. Trombelli L, Farina R. Clinical outcomes with bioactive agents alone or in combination with grafting or guided tissue regeneration. J Clin Periodontol 2008;35(8Suppl):117–135; Review.
22. Donos N, Mardas N, Chadha V. Clinical outcomes of implants following lateral bone augmentation: Systematic assessment of available options (barrier membranes, bone grafts, split osteotomy). J Clin Periodontol 2008;35(8Suppl): 173–202;Review.

TISSUE ENGINEERING: Part A
Volume 16, Number 7, 2010

DOI: 10.1089/ten.tea.2009.0585

A Sustained Release of Lovastatin from Biodegradable, Elastomeric Polyurethane Scaffolds for Enhanced Bone Regeneration

Toshitaka Yoshii, M.D., Ph.D.,[1–3] Andrea E. Hafeman, M.S.,[2,4] Jeffry S. Nyman, Ph.D.,[1,2,5] Javier M. Esparza,[2] Kenichi Shinomiya, M.D., Ph.D.,[3] Dan M. Spengler, M.D.,[1] Gregory R. Mundy, M.D.,[1,2] Gloria E. Gutierrez, M.D.,[2] and Scott A. Guelcher, Ph.D.[2,4]

Scaffolds prepared from biodegradable polyurethanes (PUR) have been investigated as a supportive matrix and delivery system for skin, cardiovascular, and bone tissue engineering. In this study, we combined reactive two-component PUR scaffolds with lovastatin (LV), which has been reported to have a bone anabolic effect especially when delivered locally, for effective bone tissue regeneration. To incorporate LV into PUR scaffolds, LV was combined with the hardener component before scaffold synthesis. The PUR scaffolds containing LV (PUR/LV) demonstrated a highly porous structure with interconnected pores, which supported *in vitro* cell attachment and proliferation and *in vivo* osteoconductive potential. The PUR/LV scaffolds showed sustained release of biologically active LV, as evidenced by the fact that LV releasates significantly enhanced osteogenic differentiation of osteoblastic cells *in vitro*. A study of bone formation *in vivo* using a rat plug defect model showed that the PUR/LV scaffolds were biocompatible. Further, locally delivered LV enhanced new bone formation in the PUR scaffolds at week 4, while there were no obvious effects at week 2. These results suggest that the sustained LV delivery system from PUR scaffolds is a potentially safe and effective device for bone regeneration.

Introduction

THE CLINICAL NEED for bone reconstruction is increasing with the substantial rise in the elderly population.[1] While autologous bone grafts have been considered the most effective procedure for treating bone defects,[2] the usefulness of autograft is limited by its supply and operative morbidity.[3] These limitations necessitate the pursuit of alternatives. In the last 10 years, there have been tremendous advances in developing synthetic and biological scaffolds for bone tissue engineering.[4–6]

Scaffolds synthesized from biodegradable polyurethanes (PUR) have recently been investigated in several tissue engineering fields, including skin,[7–9] cardiovascular,[10,11] and bone.[12,13] In these applications, PUR scaffolds have been demonstrated to support cell in-growth and tissue remodeling. PUR scaffolds have also been shown to degrade to noncytotoxic decomposition products.[7,10,14–16] In addition to inherent flexibility in processing and tunable properties, the potential to inject them as a reactive two-component liquid is an attractive feature of these materials for noninvasive therapies.[9,13] PUR scaffolds have also been studied as a drug carrier for local delivery of signaling molecules, including basic fibroblast growth factor,[17] platelet-derived growth factor (PDGF),[8,9] and bone morphogenetic protein 2 (BMP2),[18] to accelerate tissue regeneration.

Statins, natural product compounds that inhibit 3-hydroxy-3-methylglutaryl-coenzyme A (HMG-CoA) reductase and reduce serum cholesterol, have recently been reported to have pleiotropic effects on various systems, including nervous, immune, cardiovascular, and skeletal systems.[19–21] For bone, statins have been shown to increase BMP2 expression and stimulate bone formation *in vivo* and *in vitro*.[22–26] In addition to the bone anabolic effect, another advantage of statins is their lower cost of synthesis compared to recombinant BMPs.[22] Further, statins have been safely used for years in treatment of hypercholesterolemia.[27,28] Therefore, the benefits of statins for treating bone injuries have increasingly generated interest among researchers and clinicians.[29–32]

[1]Department of Orthopaedics and Rehabilitation, and [2]Center for Bone Biology, Vanderbilt University Medical Center, Nashville, Tennessee.
[3]Section of Orthopaedic and Spinal Surgery, Graduate School, Tokyo Medical and Dental University, Tokyo, Japan.
[4]Department of Chemical and Biomolecular Engineering, Vanderbilt University, Nashville, Tennessee.
[5]Department of Veterans Affairs, Tennessee Valley Healthcare System, Nashville, Tennessee.

A major limitation in the clinical application of statins for bone regeneration is an appropriate delivery system. Statins are not effective enough in stimulating bone formation when given orally, because they are subject to first-pass metabolism in liver and thus do not reach sufficient concentrations at bone sites.[27] Therefore, local application of statins may be preferable for effective bone tissue repair. However, they disperse quickly and have short half-lives[22] when injected locally. Local application of statins with high doses may cause side effects, such as cytotoxicity or an adverse inflammatory response.[33,34] Therefore, a suitable delivery system is required to optimize their efficacy for bone regeneration.

In previous studies, Whang *et al.* demonstrated sustained release kinetics of simvastatin *in vitro* by grafting the statin to the hydrolytically degradable poly(lactide-*co*-glycolide).[35] Benoit *et al.* also synthesized a poly(ethylene glycol) (PEG) hydrogel-derived delivery system for fluvastatin and showed that the released fluvastatin induced osteogenic differentiation *in vitro*.[36] In other studies, Garrett *et al.* showed that locally delivered lovastatin (LV) from poly-(DL-lactide) nanoparticles (mean particle size ~200 nm) enhanced fracture repair.[37] Jeon *et al.* reported that controlled release of simvastatin hydroxyacid from microsphere composed of a blend of cellulose acetatephthalate and a poly(ethylene oxide) and poly(propyleneoxide) block copolymer enhanced bone formation in calvarial onlay model in rats.[38] However, release of statins from synthetic polymeric porous scaffolds for *in vivo* bone regeneration has yet to be investigated. In this study, we incorporated LV particles into PUR scaffolds using a reactive liquid molding process. We used PUR scaffolds as both a delivery system for LV in an active form for enhancing osteogenesis, and also to provide a suitable matrix for the newly formed bone. In a series of *in vitro* experiments, the release profile of LV, the biocompatibility of PUR scaffolds containing LV, and the osteogenic potential of LV released from PUR scaffolds were investigated. The effects of locally delivered LV from PUR scaffolds on *in vivo* bone formation were subsequently investigated in a rat femoral plug model.

Materials and Methods

Materials

Glycolide and D,L-lactide were obtained from Polysciences, tertiary amine catalyst (TEGOAMIN33) from Goldschmidt, and glucose from Acros Organics. Lysine triisocyanate (LTI) was purchased from Kyowa Hakko USA. LV was obtained from Stason Pharmaceuticals Incorporated, and α-minimal essential medium for cell culture was purchased from Fisher Scientific. All other reagents were purchased from Sigma-Aldrich.

Synthesis of PUR scaffolds

Trifunctional polyester polyols of 900-Da molecular weight were prepared from a glycerol starter; 60% ε-caprolactone, 30% glycolide, and 10% D,L-lactide monomers; and stannous octoate catalyst.[14,15] The components were mixed in a 100-mL reaction flask with mechanical stirring under argon for 36 h at 140°C, and the resulting polyol was subsequently washed with hexane and dried under vacuum at 80°C for 14 h. PUR scaffolds were synthesized by reactive liquid molding of LTI and a hardener comprising the polyol, 1.5 parts per hundred parts polyol (pphp) water, 1.5 pphp TEGOAMIN33 tertiary amine catalyst, 1.5 pphp sulfated castor oil stabilizer, and 4.0 pphp calcium stearate pore opener. The isocyanate was added to the hardener and mixed for 30 s in a Hauschild SpeedMixer™ DAC 150 FVZ-K vortex mixer (FlackTek, Inc.). The resulting reactive liquid mixture was allowed to rise freely for 10–20 min.[14,15] The targeted index (the ratio of NCO to OH equivalents times 100) was 115. Scanning electron microscopy (SEM; Hitachi S-4200 SEM) was utilized to observe the internal pore morphology of the PUR scaffolds. The pore size distribution was determined from SEM images of multiple PUR scaffold replicates.

Incorporation of LV in PUR scaffolds and in vitro *release of LV*

To incorporate LV into PUR scaffolds (PUR/LV scaffolds), LV particles were added to the hardener component before mixing with the isocyanate. Powdered LV was mixed thoroughly with the hardener at 20 μg (low dose) and 200 μg (high dose) per gram of foam. Triplicate scaffold samples were added to 5 mL each of phosphate-buffered saline (PBS), and LV was allowed to release over time at 37°C. At each time point, the release medium was collected and replaced with fresh PBS to approximate sink conditions. LV release was quantified daily from 1 to 30 days using high-performance liquid chromatography (Waters Breeze HPLC). Fifty microliters of each sample was filtered and injected into the HPLC. Releasates were passed through an XTerra reverse-phase guard column (C8 5-μm 3.9×20 mm) and XTerra reverse-phase column (C18 5-μm 4.6×250 mm) at a flow rate of 1.0 mL/min and analyzed at 237 nm. The mobile phases, at a ratio of 50/50 (A/B), were as follows: (1) 10 mM ammonium formate (pH 4.0) and isopropyl alcohol (95/5), and (2) 10 mM ammonium formate (pH 4.0) and acetonitrile (5/95). Both were filtered through a 0.2 μm filter and degassed under vacuum. The concentration of LV was calculated from peak area by injecting samples of known concentration and preparation of a standard curve correlating concentration with peak area.

In vitro *biocompatibility of PUR/LV scaffolds*

The *in vitro* biocompatibility of PUR and PUR/LV scaffolds was evaluated using MC3T3-E1 embryonic mouse osteoblast precursor cells. Considering that previous studies have demonstrated the *in vitro* biocompatibility of PUR scaffolds,[14,15] short-term studies (up to 5 days) were performed to determine whether the LV initially released from the scaffolds had any cytotoxic effects. MC3T3-E1 cells were statically seeded onto foam discs (9×1 mm) at 5×10^4 cells per well in 24-well tissue-culture polystyrene plates. Cells were cultured with α-minimal essential medium (Fisher Scientific) containing 10% fetal bovine serum (HyClone), and 1% penicillin/streptomycin (HyClone) at 37°C in a humidified incubator supplemented with 5% CO_2. The medium was changed every 2 days. After 5 days, the cell-seeded scaffolds were removed from culture, washed with PBS, and transferred to a new 24-well plate to verify cell adherence to the materials. About 4 μM calcein AM (Invitrogen–Molecular

Probes Live/Dead Viability/Cytotoxicity Kit) was added to the samples. Calcein AM dye is retained within live cells, imparting green fluorescence (excitation/emission: 495/515 nm). Cell viability was assessed qualitatively by fluorescent images acquired with an Olympus DP71 camera attached to a fluorescent microscope (Olympus CKX41, U-RFLT50).

In addition, cell attachment, viability, and proliferation were quantified using the MTT (3-[4,5-dimethylthiazol-2-yl]-2, 5-diphenyltetrazolium bromide) assay from Sigma-Aldrich.[39,40] For the attachment study, the samples were incubated for 4 h at 37°C with 5% CO_2 to allow the cells to attach to the scaffold after cell seeding. The same number of cells was plated on the polystyrene plates as a control, and cell attachment to the scaffolds was evaluated as a relative value to the control. For the viability/proliferation assay, the cells were cultured in the scaffolds for 2 and 5 days after seeding. The scaffolds were subsequently washed with PBS and transferred to a new 24-well plate. MTT solution was added to each well and incubated at 37°C for 4 h. The insoluble formazan crystals were dissolved in dimethyl sulfoxide, and the absorbance was measured at 590 nm in a microplate reader (ELX 800; Bio-Tek) with a reference wavelength at 620 nm.

Effect of LV delivery on osteogenic differentiation in vitro

The effects of LV released from PUR scaffolds (r-LV) on osteogenic differentiation were evaluated *in vitro* using MC3T3-E1 cells. Samples of released LV were obtained from the buffer in which the PUR/LV materials were incubated for the *in vitro* LV release assay; the concentration was adjusted by diluting in cell culture medium. MC3T3-E1 cells were treated with r-LV (1 μM) and fresh LV (1 μM) was used as a positive control. In general, since the concentrations of LV in the release samples were several orders of magnitude greater than the concentration needed for *in vitro* studies, the medium composition was not altered significantly. Osteogenic medium containing 2.5% fetal bovine serum, 5 mM β-glycerophosphate (Sigma-Aldrich), and 100 μg/mL ascorbic acid phosphate (Wako) was used for mineralization assays.

BMP2 expression. Cells were plated at 2×10^5 cells/well in six-well plates and treated with either r-LV or exogenous LV for 24 h ($n=4$). Total RNA was isolated using TriZOL reagent, and mRNA was transcribed to cDNA using Superscript II (Invitrogen). Quantitative PCR of mouse BMP2 mRNA was performed using the cDNA template and mouse BMP2 TaqMan primers/probe (Mm01340178_m1; Applied Biosystems) on the 7300 real-time PCR system (Applied Biosystems). Eukaryotic 18S rRNA detected using a VIC-MGB probe (4319413E; Applied Biosystems) served as an endogenous control.[41]

Alkaline phosphatase activity. Cells were plated at 2.5×10^4 cells/well in 48 wells and treated with either r-LV or exogenous LV for 3 and 7 days. Cells were washed with PBS and lysed with 0.1% Triton X-100. The plates were then subjected to three freeze–thaw cycles. The lysates (20 μL) were added to 100 μL of substrate buffer (2 mg/mL disodium *p*-nitrophenylphosphate hexahydrate and 0.75 M 2-amino-2-methyl-1-propanol). After incubation of the mixtures at 37°C for 30 min, absorbance at 405 nm was measured. Alkaline phosphatase activity (ALP) activity was determined from a standard curve generated by employing the reaction of a *p*-nitrophenyl solution. The ALP activity was normalized by the total protein content determined using the BCA assay (Pierce).

Mineralization assay. Cells were plated at 5×10^4 cells/well in 24 wells and treated with either r-LV or exogenous LV in the osteogenic medium for 25 days. After cells were washed with PBS and fixed with 10% phosphate-buffered formalin, mineralized nodule formation was evaluated by Von Kossa staining, wherein 5% silver nitrate solution was added to the well under incandescent light for 20–45 min. After granules developed, the silver nitrate was removed, and wells were washed with water to stop the reaction. Mineralized nodule formation was assessed by capture of digital images (4×) with an Olympus DP71 camera. The fractional area in the digital images taken from four regions per sample was evaluated using ImageJ software (NIH) and the average value calculated from $n=4$ replicates.

Effect of local LV delivery from PUR scaffolds on in vivo *bone formation*

Effect of local LV delivery from PUR scaffolds on bone formation *in vivo* was evaluated using a rat plug defect model.[42] All surgical procedures were reviewed and approved by the Institutional Animal Care and Use Committee. Male Sprague-Dawley rats (Harlan Labs) aged 8 weeks (200–250 g) were used for this study. A monocortical plug bone defect (3 mm) was created in the distal region of the femur diaphysis, and cylindrical PUR scaffolds (3×5 mm) were implanted into the defect. Treatment groups included PUR (without LV as a control), PUR/LV containing 100 μg LV (LV-H), and PUR/LV containing 25 μg of LV (LV-L) ($n=6$). After 2 and 4 weeks postimplantation, the rats were sacrificed, and the femurs removed and fixed in 10% phosphate-buffered formalin.

Quantitative 3D analysis of bone formation in the scaffolds was performed using a μCT40 (SCANCO Medical) at a voxel size of 24 mm (isotropic). The X-ray source settings were 55 kVp and 145 mA with an integration time of 300 ms. The region of interest (100 axial slices) was centered over the defect site in the distal femur. After reconstruction, the bone tissue was distinguished from air or soft tissue using a threshold of 270 per thousand (or 438.7 mgHA/cm^3), a Gaussian noise filter of 0.8, and support of 2. This threshold was consistent through all specimens. Utilizing Scanco evaluation software, the amount of bone formation in the scaffold was quantified as the ratio of bone volume per total volume, in which total volume was generated by measuring the contour of the defect site. Because the μCT40 is calibrated to known densities of hydroxyapatite (phantom), the mineral density (mgHA/cm^3) of each voxel was automatically provided for segmented bone. We evaluated the mean volumetric bone density of the mineralized tissue.

Rat bones were then decalcified with 10% ethylenediaminetetraacetic acid (Invitrogen), dehydrated, embedded in paraffin, and sectioned at 5 μm thickness. The coronal slice sections were stained with hematoxylin and eosin. Specimens were examined under light microscopy. For histomorphometric

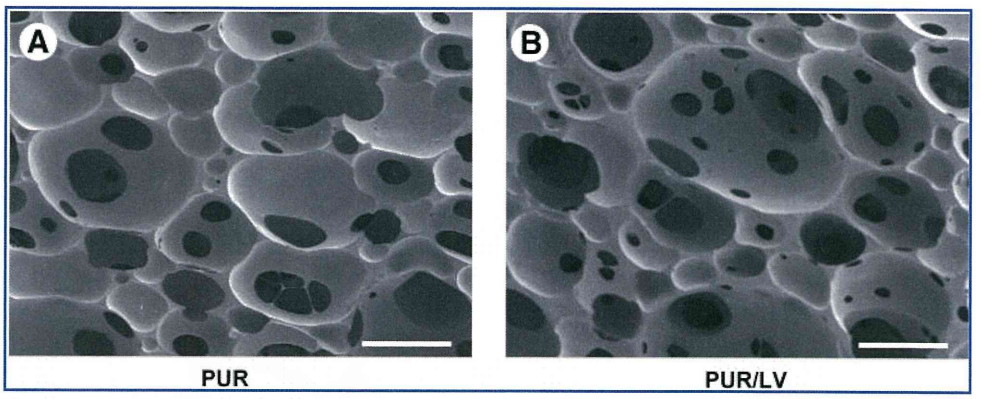

FIG. 1. Scanning electron microscope images. (**A**) Polyurethane (PUR) scaffolds and (**B**) PUR scaffolds incorporating lovastatin (PUR/LV: 200 μg LV/gram of foam). Scale bars: 250 μm.

examination, the amount of new bone formation in the scaffolds and the residual scaffolds were quantified at the center sections of the samples.[43] The newly formed bone and polymer scaffold remnants at the defect site were highlighted using image-editing software (Photoshop; Adobe Systems Incorporated) and measured using image-analysis software (Scion Image; Scioncorporation), and the ratio of new bone formation and implant per whole scaffold area was evaluated.

Statistics

Average values were expressed as the mean ± standard deviation. One-way analysis of variance and Bonferroni/Dunn *post hoc* test were used for statistical analysis. *p*-Values < 0.05 were considered significant.

Results

Synthesis of PUR scaffolds

Porous PUR scaffolds synthesized by reactive liquid molding exhibited porous structure as evidenced by SEM imaging (Fig. 1A). The pores were ellipsoidal, and the pore diameter was in the range of 200–500 μm. The thickness of the pore walls and struts was less than ~100 μm. The incorporation of LV did not obviously change the pore morphology (Fig. 1B); SEM images showed that PUR/LV (high dose) exhibited ellipsoidal pores in the same size range as the blank scaffold. Powdered LV incorporated in PUR scaffolds was not clearly visible in SEM images because of the small particle size compared to the thickness of the pore walls.

In vitro *release profile of LV from PUR scaffolds*

The amounts of LV released from PUR scaffolds *in vitro* were measured using HPLC and the cumulative% release of LV is shown in Figure 2. LV was released in a slow, sustained manner with a nearly linear release profile and a constant daily elution in both doses. Approximately 20% of LV was released from the scaffolds that contained high dose of LV in 30 days, and 10% of LV was released from the scaffolds with low dose of LV.

In vitro *biocompatibility of PUR/LV scaffolds*

Fluorescent micrographs of MC3T3-E1 osteoblastic cells cultured on PUR/LV scaffolds after 5 days are shown in Figure 3A–C. The green viable cells, as indicated by dye uptake, were easily distinguished from the autofluorescent scaffold material. The osteoblastic cells infiltrated the porous structure of the scaffold and adhered to the pore walls in all three treatment groups.

An MTT assay was also performed to quantify osteoblastic cell attachment, viability, and proliferation on the scaffolds. There were no significant differences among the treatment groups in the attachment of cells to the scaffolds after 4 h of incubation (Fig. 3D). When the cells were cultured on the scaffolds for 2 and 5 days, the MTT assay showed that the number of cells substantially increased from day 2 to 5, suggesting that the cells proliferated in all three materials (Fig. 3E). There were no differences among the treatment groups in the number of viable cells at each time point. These results suggest that PUR scaffolds are biocompatible and the incorporation of LV did not affect cell viability or proliferation on the scaffolds in osteoblastic cell culture.

Effect of LV delivery on osteogenic differentiation in vitro

To verify the bioactivity of released LV from PUR scaffolds, the effects of released LV on *BMP2* gene expression and osteoblastic differentiation were examined in monolayer culture of MC3T3-E1 osteoblastic cells. Cells were cultured with released LV on tissue culture polystyrene, rather than directly on PUR/LV scaffolds, since LV release rates *in vitro* were not be sufficiently high at this experimental timescale to initiate the biological effect of LV. As shown in Figure 4A,

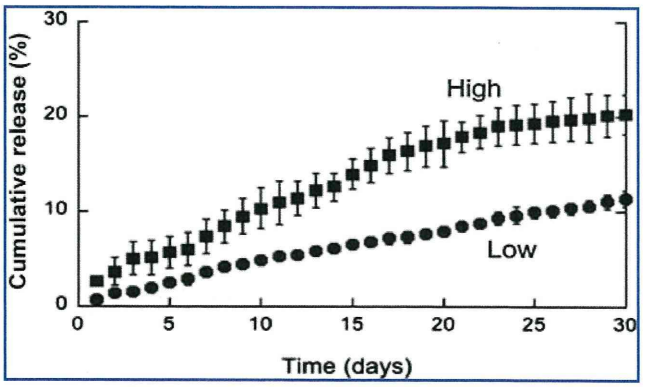

FIG. 2. *In vitro* release kinetics of LV delivered from PUR scaffolds. Cumulative percent release from PUR incorporating LV at 20 μg (Low) and 200 μg (High) per gram of foam.

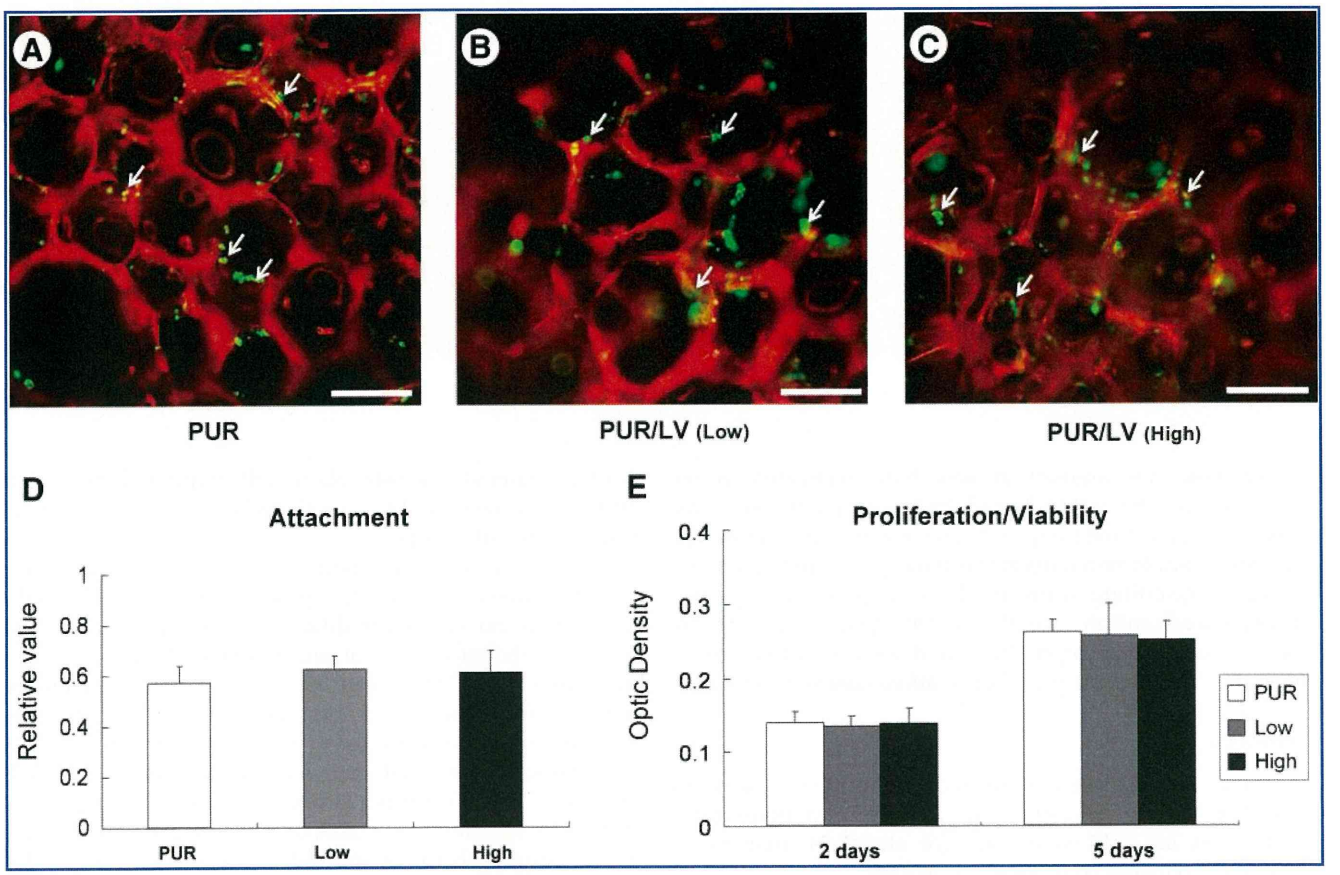

FIG. 3. *In vitro* biocompatibility of PUR/LV scaffolds. Calcein staining of viable MC3T3-E1 osteoblastic cells (green) cultured on PUR scaffolds: (**A**) PUR, (**B**) PUR/LV (Low), and (**C**) PUR/LV (High) at day 5. The arrows indicate the osteoblastic cells. Scale bars: 200 μm. Cell attachment at 4 h (**D**) and proliferation/viability at days 2 and 5 (**E**) were accessed using MTT assay ($n = 4$). Color images available online at www.liebertonline.com/ten.

BMP2 expression in the osteoblastic cells treated with LV releasates was twofold higher than that in the control. LV released from PUR scaffolds enhanced osteogenic differentiation as evidenced by ALP activity, especially at day 7 (Fig. 4B). Bone nodule formation in the cells treated with LV releasates for 25 days was also significantly enhanced when compared to the control (Fig. 4C, D). While *BMP2* gene expression, *ALP* expression, and bone nodule formation were somewhat higher for fresh LV (positive control) compared to released LV, the differences were not statistically significant, which suggests that the stimulatory potential of LV on osteogenic differentiation was preserved during the chemical reaction associated with the foaming process.

Effect of local LV delivery from PUR scaffolds on in vivo *bone formation*

To evaluate the effect of local LV delivery from PUR scaffolds on *in vivo* bone formation, cylindrical PUR scaffolds were implanted into rat femoral plug defects. At week 2, μCT analysis, which measures the amount of mineralized bone formation, showed that new bone started forming mainly at the peripheral area in the materials (Fig. 5A). There were no significant differences among the groups in the amount of new bone area and bone density (Fig. 5B, C). At week 4, μCT images showed that increased bone formation was visible throughout the implants in all treatment groups (Fig. 5A). The most extensive bone formation was observed in LV-H samples. The quantitative μCT analysis at week 4 demonstrated that the volume of new bone formation per total scaffold volume was higher in LV-H samples, although the differences were not significant ($p = 0.068$) (Fig. 5B). The density of newly formed bone in LV-H samples was significantly higher than that observed in the control PUR scaffolds at 4 weeks (Fig. 5C).

In the histological analysis, substantial cellular infiltration was observed in all groups at week 2, and new bone formation started mainly near the bottom surface of the implant (Fig. 6A). At week 4, an increased amount of mature bone formation was observed throughout the entire area of the implants (Fig. 6B). New bone formation in the scaffold was most extensive in the LV-H materials (Fig. 6C), which is consistent with the μCT analysis. The implants at week 4 had more extensively degraded in all treatment groups when compared to the samples at week 2. Although histomorphometric analysis showed no differences among groups in the area of new bone formation at week 2, LV-H samples showed significantly greater bone formation at week 4 than the control group (Fig. 6D). A significant difference in new bone formation was measured at 4 weeks for the LV-H treatment group by histomorphometry, but not by μCT. This difference in outcomes between the two experimental

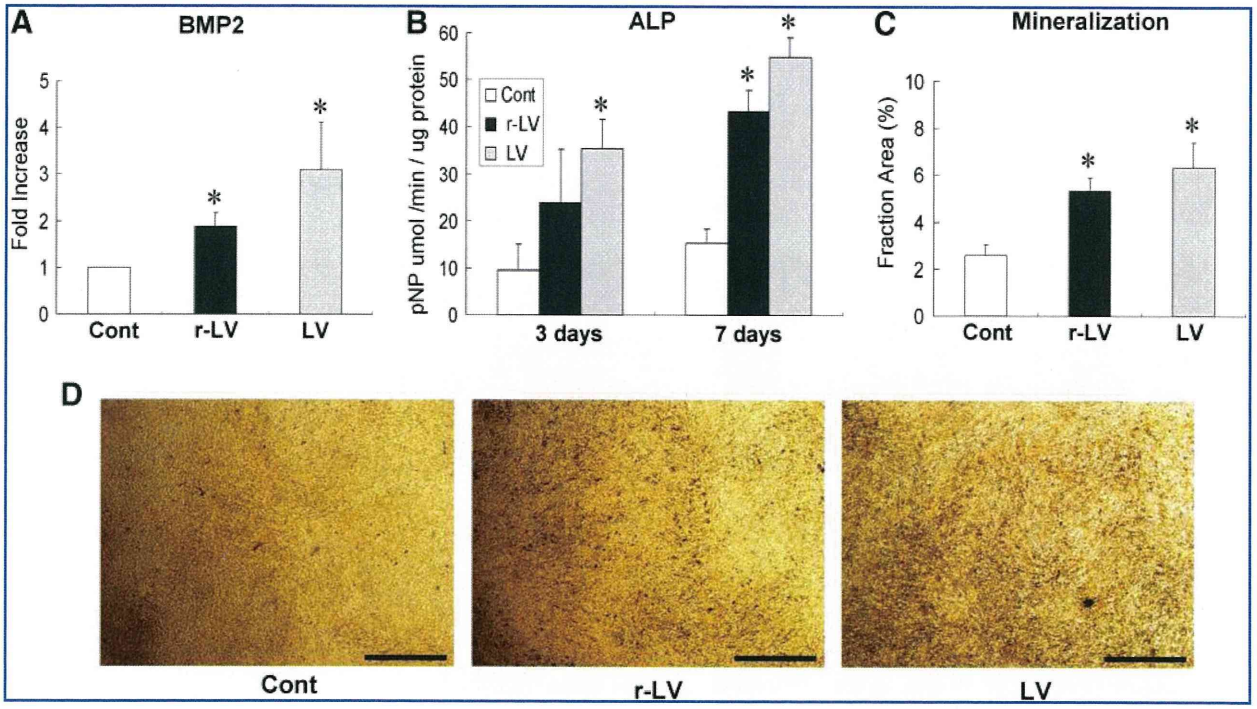

FIG. 4. Effect of LV delivery on osteogenic differentiation *in vitro*. MC3T3-E1 osteoblastic cells were treated with LV releasates from PUR scaffolds (r-LV). Fresh LV was used as a positive control (LV). (**A**) Bone morphogenetic protein 2 (BMP2) expression, (**B**) alkaline phosphatase activity (ALP) activity, and (**C, D**) mineralized nodule formation (Von Kossa staining) were evaluated ($n = 4$). Scale bars: 1 mm. $^*p < 0.05$ versus control. Color images available online at www.liebertonline.com/ten.

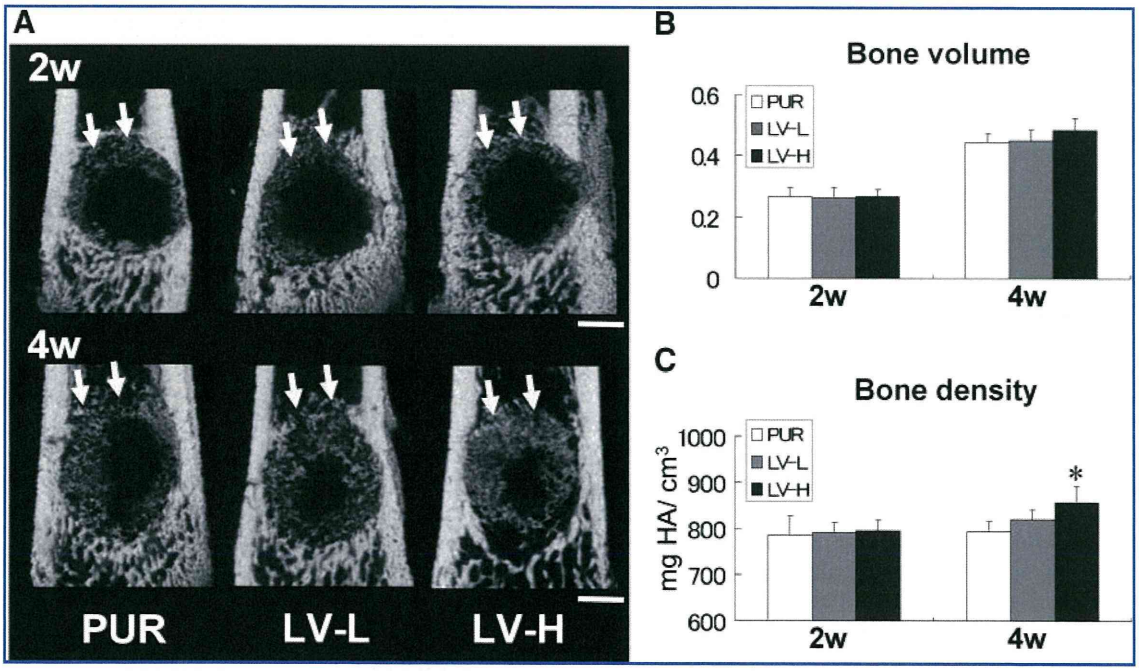

FIG. 5. Effect of local LV delivery from PUR scaffolds on *in vivo* bone formation. The PUR and PUR/LV scaffolds were implanted into rat femoral plug defects: (**A**) representative sagittal μCT images at 2 and 4 weeks postimplantation. Arrows highlight areas of new bone formation. Scale bars: 1 mm. Quantitative analysis of mineralized new bone formation: (**B**) bone volume per total volume of implants and (**C**) mean bone density ($n = 6$). $^*p < 0.05$ versus PUR.

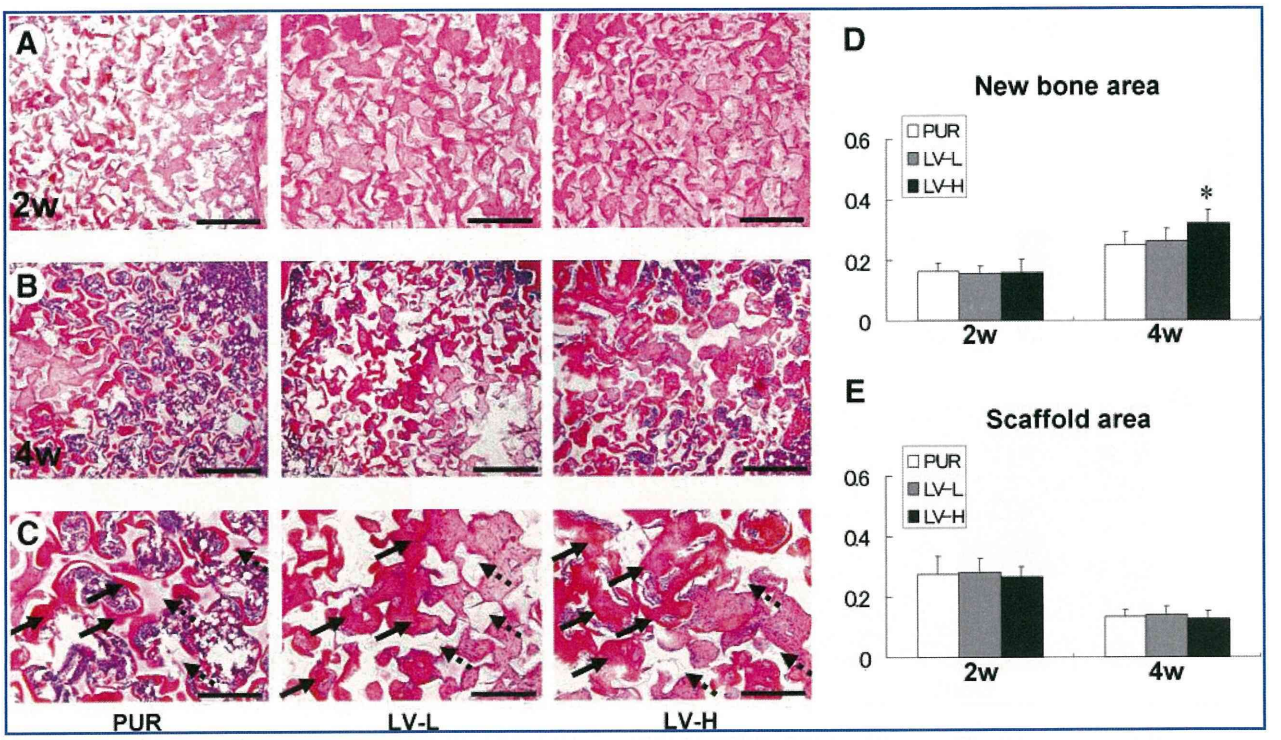

FIG. 6. Histological evaluation of *in vivo* bone formation study. Representative decalcified histological sections (hematoxylin and eosin) at (**A**) 2 weeks and (**B**) 4 weeks postimplantation (coronal). Scale bars: 1 mm. (**C**) High magnification of the sections at 4 weeks. Solid arrows indicate newly formed bone and dotted arrows indicate residual scaffolds. Scale bars: 250 μm. The area of (**D**) new bone formation and (**E**) scaffolds in the histological sections was evaluated ($n = 6$). *$p < 0.05$ versus PUR. Color images available online at www.liebertonline.com/ten.

techniques could be attributed to the fact that the histomorphometric analysis includes both mineralized bone as well as bone matrix that is not fully mineralized, whereas the μCT analysis includes only mineralized bone. In all groups, the residual scaffold area at week 4 was nearly half that of the samples at week 2; there were no significant differences among treatment groups both at weeks 2 and 4 (Fig. 6E).

Discussion

Biodegradable PUR materials have been investigated in tissue engineering as supportive scaffolds for cell attachment, growth, and differentiation. Recent studies have shown that scaffolds fabricated from biodegradable segmented PUR elastomers comprising hexamethylene diisocyanate supported infiltration of cells and bone ingrowth when implanted in defects in the iliac crest of sheep.[12,44] Similarly, two-component lysine diisocyanate-based PUR biomaterials incorporating β-tricalcium phosphate showed bone ingrowth in femoral defects in sheep.[13] In this study, we used a high-porosity LTI-based PUR scaffold with resilient elastomeric mechanical properties.[9] The material has an ellipsoidal pore structure with interconnected pores, which supported cell attachment and growth in osteoblastic cell culture *in vitro*. In a previously reported cell culture study, MC3T3 cells were observed to migrate into the interior of the PUR scaffolds for up to 21 days, suggesting that the pores were interconnected.[15] In this *in vivo* study, cellular infiltration and ingrowth of new bone into the materials were observed as early as 2 weeks, with increased new bone formation at 4 weeks. These results suggest that the LTI-based two-component PUR scaffolds exhibit interconnected pores and demonstrate osteoconductive properties, which is in agreement with previous studies.

Since the original report describing the effects of statins in bone,[22] there have been multiple publications confirming the effects of these drugs in bone cells and many other studies looking at their mechanism of action. Statins known to inhibit the mevalonate pathway induce *BMP2* gene expression, which in turn initiates a cascade of events that ultimately stimulates osteoblasts. *BMP2* is one of the most potent osteoinductive agents involved in recruitment, proliferation, and differentiation of osteoprogenitor cells, resulting in bone formation. Considering that statins are rapidly absorbed after oral administration and their systemic bioavailability is low,[27] administering these drugs locally to defect sites was anticipated to be a more effective strategy for bone regeneration than systemic delivery.

It is intriguing that statins, drugs that are believed to primarily stimulate osteoblastic bone formation, and bisphosphonates, compounds that are well-established inhibitors of osteoclastic bone resorption, have targets in the same metabolic pathway, the mevalonate pathway of cholesterol biosynthesis. Although some studies (including the original publication) have shown statins to also affect osteoclastic bone resorption, the major effect of statins is bone formation. The actions of statins in bone can be abolished when noggin, a naturally occurring inhibitor of BMP2, is added to bone cells. It has also been demonstrated that bone formation *in vivo* is impaired in transgenic mice that have a truncated

dominant-negative type receptor (BMPR-IB) targeted to osteoblasts,[45] confirming again the importance of BMP2 as a mediator of the statin effect in bone formation. On the other hand, bisphosphonates are strong bone resorption inhibitors, although recently they have also been shown to stimulate osteoblastic bone formation.[46–48]

The fact that both statins and bisphosphonates have targets in the same metabolic pathway results in concerns regarding complications due to potential interactions between the two drugs. However, although both drug classes prevent the prenylation of guanosine triphosphate (GTP)-binding proteins, the pharmacological mechanism of action in aminobisphosphonates is based on interference with the mevalonate pathway by inhibiting the more downstream farnesyl pyrophosphate synthase enzyme, while statins act far upstream on the mevalonate pathway by inhibiting the HMG-CoA reductase. Therefore, these two drug classes interfere with distinct pathways branching from the main mevalonate pathway, and are linked to the different levels of the mevalonate pathway. Moreover, bisphosphonates preferentially bind to the surface of bone at sites of active remodeling and become internalized into osteoclasts via endocytosis, which might explain why their effects on the mevalonate pathway are much more apparent in osteoclasts. Further, bisphosphonates have been shown recently to induce formation of a novel ATP analog (Apppl) as a consequence of inhibition of the mevalonate pathway and this molecule has been shown to cause apoptosis in osteoclasts.[48] Since statins inhibit this pathway far upstream, the levels of Apppl are decreased, which might explain the different effects of both drugs. Local delivery of statins in patients taking bisphosphonates is thus not anticipated to have a detrimental effect or cause bisphosphonate-associated osteonecrosis for the above-mentioned differences in the mechanism of action. However, more detailed studies are required to determine any potential interactions between statins and bisphosphonates.

Local drug delivery achieved through incorporation of signaling molecules in a scaffold is an established and effective approach to regenerating tissue.[49,50] PUR scaffolds have been shown to deliver basic fibroblast growth factor,[17] rhPDGF-BB,[8] and rhBMP2.[18] In this study, we incorporated LV into PUR scaffolds for local delivery to bony sites by mixing it in powder form with the polyol-based hardener component before polymerization with LTI. We have previously shown that the biological activity of molecules that have active hydrogen (e.g., hydroxyl and amine) groups, such as tobramycin and PDGF, was not adversely affected by the PUR reaction when incorporated as solid particles.[8,51] In contrast, when a molecule with active hydrogen groups was added to the two-component formulation as an aqueous solution, the release was almost negligible due to covalent bonding between the bioactive molecule and the PUR.[51] The encapsulation of LV particles did not noticeably affect the morphology of the PUR scaffolds, as shown by SEM analysis. The highly porous structure with interconnected pores, which supported cell attachment and growth, was preserved well in the PUR scaffolds even with LV incorporation. As a result, PUR/LV scaffolds demonstrated equal potential for osteoblastic cell attachment and proliferation *in vitro* as PUR scaffolds without LV. PUR/LV and PUR scaffolds also showed similar abilities to allow cell infiltration to the scaffolds *in vivo* at 2 weeks postimplantation.

To deliver statins safely and effectively to the wound site, a sustained local delivery system is preferred to systemic delivery. An initial burst release of statins raises cytotoxicity concerns due to the dramatically reduced production of cholesterol, a molecule required for membrane integrity. Further, an adverse inflammatory response has been reported after local administration of high doses of statins *in vivo*.[33,34] In the present study, LV release from PUR scaffolds followed a sustained and linear profile, thus minimizing the potentially negative side effects of locally high statin concentrations. The burst release was <3%, and after the 30 days the cumulative release varied from 12% to 22%. These data are in agreement with a previous study investigating the release of simvastatin (which also has very low water solubility) from poly(lactic-*co*-glycolic acid) (PLGA) scaffolds, where the burst release was 5% and the cumulative release at 30 days was 32%.[35] Release of LV particles from PUR scaffolds is thus conjectured to be diffusion-controlled, as reported previously for simvastatin particles embedded in PLGA scaffolds. Due in part to the low water solubility of LV (0.4 μg/mL), the diffusion-controlled release occurs slowly, and under *in vitro* conditions is primarily independent of PUR degradation, considering that the degradation time of these materials is on the order of weeks to months.[51] The higher cumulative release of LV observed at the high dose relative to the low dose (Fig. 1C) is conjectured to result from the formation of channels created by LV, which has already diffused away from the interior of the scaffold.[52] Thus, a higher LV loading is anticipated to create more (or larger) channels for LV diffusion from the polymer, resulting in accelerated release kinetics. Previously, we have shown that a hydrophilic drug with high water solubility, such as tobramycin, is released much faster from PUR scaffolds with an initial burst release >30%.[51] The release rate can be accelerated slightly by incorporating PEG, which increases the hydrophilicity and swelling of the PUR scaffold (LV data not shown).[51] Faster release rates of statins have been achieved through other approaches, such as encapsulation of LV in nanospheres 50–350 nm in diameter, which exhibited a minimal burst release and 25% cumulative release after 10 days, presumably due to the relatively short diffusion path.[37] While encapsulation of LV in 50–350 nm nanoparticles has been shown to achieve more efficient release kinetics, we have previously shown that incorporation of ~1 μm microspheres in a PUR scaffold substantially reduced the rate of release relative to the microspheres alone. In contrast, scaffolds incorporating ~100 μm microspheres exhibited release kinetics comparable to that of the microspheres alone.[18] This reduction in release kinetics observed for small (<1 μm) particles embedded in the scaffolds was attributed to the increased resistance to mass transfer resulting from the pore walls. In another study, fluvastatin (which has substantially higher water solubility than LV) tethered to a PEG hydrogel by a degradable lactic acid spacer–exhibited tunable release kinetics, with 100% cumulative release after 7–40 days *in vitro*.[36] The faster release kinetics observed for the fluvastatin hydrogel delivery system is attributed to the degradation-controlled release mechanism in contrast to the diffusion-controlled mechanism associated with the PUR scaffolds.

The scaffolds both with and without LV exhibited biocompatibility when cultured with osteoblastic cells *in vitro*.

While the PUR scaffolds were not directly compared to other materials in this study, previous studies have shown that the lysine polyisocyanate-derived PUR scaffolds support cellular attachment and proliferation comparably to other polymeric biomaterials, including tissue culture polystyrene, PLGA, and polyethylene for periods up to 21 days.[14,15] Histological analysis demonstrated substantial degradation of PUR scaffolds at week 4 *in vivo*, which is in agreement with previous studies demonstrating the PUR scaffolds degrade to non-cytotoxic decomposition products.[9,53] None of the histological sections showed severe inflammation, suggesting that neither the PUR degradation products nor the released LV induced an adverse inflammatory response for the LV doses used in this study. In a previous study, rats treated with simvastatin in a methylcellulose gel on the lateral aspect of the mandible exhibited 45% more bone formation and reduced clinical swelling when the simvastatin dose was reduced from 2.2 mg to 500 μg.[33] These facts suggest that the PUR/LV sustained delivery system can be used safely for bone tissue repair by delivering LV doses that are high enough to promote new bone formation but below the threshold for inflammation.

On the basis of the fact that LV needs to be converted to the hydrophilic acid form to become biologically active,[54] we examined the effect of LV released from PUR scaffolds on osteogenesis *in vitro* to verify the bioactivity of the released compounds. These experiments were designed to determine whether the biological activity of LV was adversely affected by the PUR reaction. Induction of osteogenic differentiation and mineralization, as evaluated by ALP activity and mineralized nodule formation, resulted when MC3T3-E1 osteoblastic cells were cultured with LV releaseates. Osteogenic differentiation in MC3T3-E1 osteoblastic cells is promoted by simvastatin through increased BMP2 expression.[24,25] Similarly, the enhanced ALP activity and mineralized nodule formation in this study is attributed to increased expression of BMP2 caused by LV releasates, suggesting that LV is released from PUR scaffolds in an active form and the stimulatory osteogenic effect by promoting BMP2 production is thus preserved. Since the osteogenic potential of BMP2 is well known to be beneficial for fracture repair and regenerating bone defects,[55–57] delivery of bioactive LV with PUR scaffolds can be useful for bone regeneration.

In clinical settings, defects in long bone caused by pathological or traumatic conditions (e.g., bone tumors, infections, or major trauma) often require reconstruction using bone substitutes.[58] To evaluate the anabolic effect of LV in long bone defects and investigate its utility as a bone void filler, the PUR/LV scaffolds were evaluated in a rat femoral defect model, which is highly reproducible and useful for investigating the efficacy of new materials and drugs.[18] While published reports have demonstrated the efficacy of LV for healing of fractures and defects in craniofacial bone, the effects of local delivery of LV on healing of orthopedic long bone defects are not known. We therefore reasoned that the femoral plug model was an appropriate starting point before testing the materials in more challenging critical-sized defects. The *in vivo* study demonstrated that new bone formation was enhanced by local delivery of LV from PUR scaffolds, which is consistent with several previous studies for bone defect repair using statins.[34,59,60] The biological activity of statins *in vivo* is attributed to increased production of endogenous BMP2.[61] Interestingly, there were no differences in the amount of bone formation at week 2, which contrasts with previous studies reporting new bone formation as early as day 5 in rabbit parietal bone defects treated with simvastatin delivered from a collagen sponge.[59,60] However, bone matrix formation observed in histological sections was significantly promoted by local delivery of LV at week 4. Although the difference in mineralized bone volume evaluated by μCT was not statistically significant at week 4, it is possible that the effects of LV on mineralized bone formation may extend beyond week 4. It is known that progenitor cells require time to substantially infiltrate the defect and scaffold.[62] Therefore, the effect of LV in enhancing endogenous BMP2 production may be delayed until these cells are present, at which point subsequent osteogenic differentiation and mineralization can occur. For this reason, a sustained statin release profile may be important, considering that statins could be most effective when a substantial number of cells have migrated into the scaffolds rather than during the initial few days after surgery. In our previous fracture healing study using LV, delayed percutaneous injection of LV (1 week after surgery) into the fracture site resulted in enhanced fracture repair relative to injection within 1 day in a rat model.[63] The improvement in repair associated with delayed injection was considered to result from a larger number of cells at the fracture site. In another study, simvastatin released from a calcium sulfate carrier did not enhance new bone formation at 2 and 4 weeks in critical-sized calvarial defects in rats.[34] However, at 8 weeks, the simvastatin-treated defects exhibited significantly more new bone formation relative to the calcium sulfate controls. These observations further suggest that sustained release of LV from scaffolds is important for effective bone formation.

In the non-critical-sized plug defect model used in this study, a faster release profile of an anabolic drug would likely perform better than a slower release profile for the necessarily short observation periods due to the fast healing of the defect.[18] Therefore, a larger defect model, such as a critical-sized segmental defect,[64,65] could be more suitable for longer observation periods, and thus should be considered for further examination to investigate the effects of sustained release of LV on bone formation.

Conclusions

In this study, we investigated the effects of local delivery of LV from PUR scaffolds on osteoblastic differentiation *in vitro* and new bone formation *in vivo*. At a dose of 200 μg, the LV concentration was sufficiently high to enhance new bone formation in a rat femoral plug model, but below the threshold at which adverse inflammation occurs. Further studies are required to investigate the effects of local delivery of LV on healing of more challenging wounds, such as critical-size defects. However, this study showed the potential of using statins to enhance healing of bony defects through local delivery from polymeric scaffolds.

Acknowledgments

This work was supported by the USAISR Orthopaedic Trauma Research Program and Vanderbilt University School of Engineering. The authors thank Katarzyna J. Zienkiewicz for measuring LV by HPLC.

Disclosure Statement

Gregory R. Mundy and Gloria E. Gutierrez have stock options in OsteoGenix, which own issued patents on the effects of statins on bone. None of the other authors have conflict of interests.

References

1. Lysaght, M.J., and Reyes, J. The growth of tissue engineering. Tissue Eng **7,** 485, 2001.
2. Enneking, W.F., Eady, J.L., and Burchardt, H. Autogenous cortical bone grafts in the reconstruction of segmental skeletal defects. J Bone Joint Surg Am **62,** 1039, 1980.
3. Younger, E.M., and Chapman, M.W. Morbidity at bone graft donor sites. J Orthop Trauma **3,** 192, 1989.
4. Perry, C.R. Bone repair techniques, bone graft, and bone graft substitutes. Clin Orthop Relat Res **360,** 71, 1999.
5. Finkemeier, C.G. Bone-grafting and bone-graft substitutes. J Bone Joint Surg Am **84-A,** 454, 2002.
6. Giannoudis, P.V., Dinopoulos, H., and Tsiridis, E. Bone substitutes: an update. Injury **36 Suppl 3,** S20, 2005.
7. Zhang, J.Y., Beckman, E.J., Hu, J., Yang, G.G., Agarwal, S., and Hollinger, J.O. Synthesis, biodegradability, and biocompatibility of lysine diisocyanate-glucose polymers. Tissue Eng **8,** 771, 2002.
8. Li, B., Davidson, J.M., and Guelcher, S.A. The effect of the local delivery of platelet-derived growth factor from reactive two-component polyurethane scaffolds on the healing in rat skin excisional wounds. Biomaterials **30,** 3486, 2009.
9. Hafeman, A.E., Li, B., Yoshii, T., Zienkiewicz, K., Davidson, J.M., and Guelcher, S.A. Injectable biodegradable polyurethane scaffolds with release of platelet-derived growth factor for tissue repair and regeneration. Pharm Res **25,** 2387, 2008.
10. Guan, J., Sacks, M.S., Beckman, E.J., and Wagner, W.R. Synthesis, characterization, and cytocompatibility of elastomeric, biodegradable poly(ester-urethane)ureas based on poly(caprolactone) and putrescine. J Biomed Mater Res **61,** 493, 2002.
11. Fujimoto, K.L., Guan, J., Oshima, H., Sakai, T., and Wagner, W.R. *In vivo* evaluation of a porous, elastic, biodegradable patch for reconstructive cardiac procedures. Ann Thorac Surg **83,** 648, 2007.
12. Gorna, K., and Gogolewski, S. Preparation, degradation, and calcification of biodegradable polyurethane foams for bone graft substitutes. J Biomed Mater Res A **67,** 813, 2003.
13. Adhikari, R., Gunatillake, P.A., Griffiths, I., Tatai, L., Wickramaratna, M., Houshyar, S., *et al.* Biodegradable injectable polyurethanes: synthesis and evaluation for orthopaedic applications. Biomaterials **29,** 3762, 2008.
14. Guelcher, S.A., Patel, V., Gallagher, K.M., Connolly, S., Didier, J.E., Doctor, J.S., and Hollinger, J.O. Synthesis and *in vitro* biocompatibility of injectable polyurethane foam scaffolds. Tissue Eng **12,** 1247, 2006.
15. Guelcher, S., Srinivasan, A., Hafeman, A., Gallagher, K., Doctor, J., Khetan, S., McBride, S., and Hollinger, J. Synthesis, *in vitro* degradation, and mechanical properties of two-component poly(ester urethane)urea scaffolds: effects of water and polyol composition. Tissue Eng **13,** 2321, 2007.
16. Guelcher, S.A. Biodegradable polyurethanes: synthesis and applications in regenerative medicine. Tissue Eng Part B Rev **14,** 3, 2008.
17. Guan, J., Stankus, J.J., and Wagner, W.R. Biodegradable elastomeric scaffolds with basic fibroblast growth factor release. J Control Release **120,** 70, 2007.
18. Li, B., Yoshii, T., Hafeman, A.E., Nyman, J.S., Wenke, J.C., and Guelcher, S.A. The effects of rhBMP-2 released from biodegradable polyurethane/microsphere composite scaffolds on new bone formation in rat femora. Biomaterials **30,** 6768, 2009.
19. Liao, J.K., and Laufs, U. Pleiotropic effects of statins. Annu Rev Pharmacol Toxicol **45,** 89, 2005.
20. Almuti, K., Rimawi, R., Spevack, D., and Ostfeld, R.J. Effects of statins beyond lipid lowering: potential for clinical benefits. Int J Cardiol **109,** 7, 2006.
21. Weber, M.S., Youssef, S., Dunn, S.E., Prod'homme, T., Neuhaus, O., Stuve, O., Greenwood, J., Steinman, L., and Zamvil, S.S. Statins in the treatment of central nervous system autoimmune disease. J Neuroimmunol **178,** 140, 2006.
22. Mundy, G., Garrett, R., Harris, S., Chan, J., Chen, D., Rossini, G., Boyce, B., Zhao, M., and Gutierrez, G. Stimulation of bone formation *in vitro* and in rodents by statins. Science **286,** 1946, 1999.
23. Garrett, I.R., Gutierrez, G., and Mundy, G.R. Statins and bone formation. Curr Pharm Des **7,** 715, 2001.
24. Maeda, T., Matsunuma, A., Kawane, T., and Horiuchi, N. Simvastatin promotes osteoblast differentiation and mineralization in MC3T3-E1 cells. Biochem Biophys Res Commun **280,** 874, 2001.
25. Maeda, T., Matsunuma, A., Kurahashi, I., Yanagawa, T., Yoshida, H., and Horiuchi, N. Induction of osteoblast differentiation indices by statins in MC3T3-E1 cells. J Cell Biochem **92,** 458, 2004.
26. Baek, K.H., Lee, W.Y., Oh, K.W., Tae, H.J., Lee, J.M., Lee, E.J., Han, J.H., Kang, M.I., Cha, B.Y., Lee, K.W., Son, H.Y., and Kang, S.K. The effect of simvastatin on the proliferation and differentiation of human bone marrow stromal cells. J Korean Med Sci **20,** 438, 2005.
27. Schachter, M. Chemical, pharmacokinetic and pharmacodynamic properties of statins: an update. Fundam Clin Pharmacol **19,** 117, 2005.
28. Armitage, J. The safety of statins in clinical practice. Lancet **370,** 1781, 2007.
29. Mundy, G.R. Statins and their potential for osteoporosis. Bone **29,** 495, 2001.
30. Gonyeau, M.J. Statins and osteoporosis: a clinical review. Pharmacotherapy **25,** 228, 2005.
31. Gutierrez, G.E., Lalka, D., Garrett, I.R., Rossini, G., and Mundy, G.R. Transdermal application of lovastatin to rats causes profound increases in bone formation and plasma concentrations. Osteoporos Int **17,** 1033, 2006.
32. Toh, S., and Hernandez-Diaz, S. Statins and fracture risk. A systematic review. Pharmacoepidemiol Drug Saf **16,** 627, 2007.
33. Stein, D., Lee, Y., Schmid, M.J., Killpack, B., Genrich, M.A., Narayana, N., *et al.* Local simvastatin effects on mandibular bone growth and inflammation. J Periodontol **76,** 1861, 2005.
34. Nyan, M., Sato, D., Oda, M., Machida, T., Kobayashi, H., Nakamura, T., and Kasugai, S. Bone formation with the combination of simvastatin and calcium sulfate in critical-sized rat calvarial defect. J Pharmacol Sci **104,** 384, 2007.
35. Whang, K., McDonald, J., Khan, A., and Satsangi, N. A novel osteotropic biomaterial OG-PLG: synthesis and *in vitro* release. J Biomed Mater Res A **74A,** 237, 2005.
36. Benoit, D.S., Nuttelman, C.R., Collins, S.D., and Anseth, K.S. Synthesis and characterization of a fluvastatin-releasing hydrogel delivery system to modulate hMSC differentiation and function for bone regeneration. Biomaterials **27,** 6102, 2006.

37. Garrett, I.R., Gutierrez, G.E., Rossini, G., Nyman, J., McCluskey, B., Flores, A., and Mundy, G.R. Locally delivered lovastatin nanoparticles enhance fracture healing in rats. J Orthop Res **25,** 1351, 2007.
38. Jeon, J.H., Piepgrass, W.T., Lin, Y.L., Thomas, M.V., and Puleo, D.A. Localized intermittent delivery of simvastatin hydroxyacid stimulates bone formation in rats. J Periodontol **79,** 1457, 2008.
39. Wutticharoenmongkol, P., Pavasant, P., and Supaphol, P. Osteoblastic phenotype expression of MC3T3-E1 cultured on electrospun polycaprolactone fiber mats filled with hydroxyapatite nanoparticles. Biomacromolecules **8,** 2602, 2007.
40. Zhang, L.F., Yang de, J., Chen, H.C., Sun, R., Xu, L., Xiong, Z.C., Govender, T., and Xiong, C.D. An ionically crosslinked hydrogel containing vancomycin coating on a porous scaffold for drug delivery and cell culture. Int J Pharm **353,** 74, 2008.
41. Zhao, M., Ko, S.Y., Liu, J.H., Chen, D., Zhang, J., Wang, B., Harris, S.E., Oyajobi, B.O., and Mundy, G.R. Inhibition of microtubule assembly in osteoblasts stimulates bone morphogenetic protein 2 expression and bone formation through transcription factor Gli2. Mol Cell Biol **29,** 1291, 2009.
42. Karp, J.M., Rzeszutek, K., Shoichet, M.S., and Davies, J.E. Fabrication of precise cylindrical three-dimensional tissue engineering scaffolds for *in vitro* and *in vivo* bone engineering applications. J Craniofac Surg **14,** 317, 2003.
43. Torigoe, I., Sotome, S., Tsuchiya, A., Yoshii, T., Maehara, H., Sugata, Y., Inchinose, S., Shinomiya, K., and Okawa, A. Bone regeneration with autologous plasma, bone marrow stromal cells, and porous beta-tricalcium phosphate in nonhuman primates. Tissue Eng Part A **15,** 1489, 2009.
44. Gorna, K., and Gogolewski, S. Biodegradable polyurethanes for implants. II. *In vitro* degradation and calcification of materials from poly(epsilon-caprolactone)-poly(ethylene oxide) diols and various chain extenders. J Biomed Mater Res **60,** 592, 2002.
45. Zhao, M., Harris, S.E., Horn, D., Geng, Z., Nishimura, R., Mundy, G.R., and Chen, D. Bone morphogenetic protein receptor signaling is necessary for normal murine postnatal bone formation. J Cell Biol **157,** 1049, 2002.
46. Im, G.I., Qureshi, S.A., Kenney, J., Rubash, H.E., and Shanbhag, A.S. Osteoblast proliferation and maturation by bisphosphonates. Biomaterials **25,** 4105, 2004.
47. Reinholz, G.G., Getz, B., Pederson, L., Sanders, E.S., Subramaniam, M., Ingle, J.N., and Spelsberg, T.C. Bisphosphonates directly regulate cell proliferation, differentiation, and gene expression in human osteoblasts. Cancer Res **60,** 6001, 2000.
48. Plotkin, L.I., Weinstein, R.S., Parfitt, A.M., Roberson, P.K., Manolagas, S.C., and Bellido, T. Prevention of osteocyte and osteoblast apoptosis by bisphosphonates and calcitonin. J Clin Invest **104,** 1363, 1999.
49. Rose, F.R., Hou, Q., and Oreffo, R.O. Delivery systems for bone growth factors—the new players in skeletal regeneration. J Pharm Pharmacol **56,** 415, 2004.
50. Drosse, I., Volkmer, E., Capanna, R., De Biase, P., Mutschler, W., and Schieker, M. Tissue engineering for bone defect healing: an update on a multi-component approach. Injury **39 Suppl 2,** S9, 2008.
51. Hafeman, A.E., Zienkiewicz, K.J., Carney, E., Litzner, B., Stratton, C.W., Wenke, J.C., and Guelcher, S.A. Local delivery of tobramycin from injectable biodegradable polyurethane scaffolds. J Biomater Sci Polym Ed **21,** 95, 2010.
52. Park, K. Controlled Drug Delivery: Challenges and Strategies. Washington, DC: American Chemical Society, 1997.
53. Guelcher, S.A., Dumas, J., Srinivasan, A., Didier, J.E., and Hollinger, J.O. Synthesis, mechanical properties, biocompatibility, and biodegradation of polyurethane networks from lysine polyisocyanates. Biomaterials **29,** 1762, 2008.
54. Alessandri, C., and Peverini, F. [Hypercholesterolemia: therapeutic approach]. Clin Ter **137,** 373, 1991.
55. Mont, M.A., Ragland, P.S., Biggins, B., Friedlaender, G., Patel, T., Cook, S., *et al.* Use of bone morphogenetic proteins for musculoskeletal applications. An overview. J Bone Joint Surg Am **86-A Suppl 2,** 41, 2004.
56. Wozney, J.M., and Rosen, V. Bone morphogenetic protein and bone morphogenetic protein gene family in bone formation and repair. Clin Orthop Relat Res **346,** 26, 1998.
57. Termaat, M.F., Den Boer, F.C., Bakker, F.C., Patka, P., and Haarman, H.J. Bone morphogenetic proteins. Development and clinical efficacy in the treatment of fractures and bone defects. J Bone Joint Surg Am **87,** 1367, 2005.
58. Paderni, S., Terzi, S., and Amendola, L. Major bone defect treatment with an osteoconductive bone substitute. Chir Organi Mov **93,** 89, 2009.
59. Wong, R.W., and Rabie, A.B. Statin collagen grafts used to repair defects in the parietal bone of rabbits. Br J Oral Maxillofac Surg **41,** 244, 2003.
60. Wong, R.W., and Rabie, A.B. Histologic and ultrastructural study on statin graft in rabbit skulls. J Oral Maxillofac Surg **63,** 1515, 2005.
61. Alam, S., Ueki, K., Nakagawa, K., Marukawa, K., Hashiba, Y., Yamamoto, E., Sakulsak, N., and Iseki, S. Statin-induced bone morphogenetic protein (BMP) 2 expression during bone regeneration: an immunohistochemical study. Oral Surg Oral Med Oral Pathol Oral Radiol Endod **107,** 22, 2009.
62. Seeherman, H., Li, R., Bouxsein, M., Kim, H., Li, X.J., Smith-Adaline, E.A., Aiolova, M., and Wozney, J.M. rhBMP-2/calcium phosphate matrix accelerates osteotomy-site healing in a nonhuman primate model at multiple treatment times and concentrations. J Bone Joint Surg Am **88,** 144, 2006.
63. Gutierrez, G.E., Nyman, J.S., Munoz, S., Jadhav, S., Yoshii, T., Esparza, J.M., and Mundy, G.R. Sustained release lovastatin applied one week after fracture accelerates healing in a rat model of fracture repair. Abstract presented at the 55th Orthopaedic Research Society Annual Meeting, Las Vegas, NV, 2009. Abstract no. 130.
64. Moore, D.C., Pedrozo, H.A., Crisco, J.J., 3rd, and Ehrlich, M.G. Preformed grafts of porcine small intestine submucosa (SIS) for bridging segmental bone defects. J Biomed Mater Res A **69,** 259, 2004.
65. Chu, T.M., Warden, S.J., Turner, C.H., and Stewart, R.L. Segmental bone regeneration using a load-bearing biodegradable carrier of bone morphogenetic protein-2. Biomaterials **28,** 459, 2007.

Address correspondence to:
Scott A. Guelcher, Ph.D.
Department of Chemical and Biomolecular Engineering
Vanderbilt University
2301 Vanderbilt Place
VU Station B #351604
Nashville, TN 37235

E-mail: scott.guelcher@vanderbilt.edu

Received: August 31, 2009
Accepted: March 4, 2010
Online Publication Date: April 5, 2010

ARTHRITIS & RHEUMATISM
Vol. 62, No. 5, May 2010, pp 1329–1337
DOI 10.1002/art.27400

Osteopontin Deficiency Impairs Wear Debris–Induced Osteolysis via Regulation of Cytokine Secretion From Murine Macrophages

Sadanori Shimizu,[1] Naoki Okuda,[1] Norihiko Kato,[2] Susan R. Rittling,[3] Atsushi Okawa,[2] Kenichi Shinomiya,[1] Takeshi Muneta,[1] David T. Denhardt,[3] Masaki Noda,[1] Kunikazu Tsuji,[4] and Yoshinori Asou[2]

Objective. **To investigate the molecular mechanisms underlying particle-induced osteolysis, we focused on osteopontin (OPN), a cytokine and cell-attachment protein that is associated with macrophage chemoattractant and osteoclast activation.**

Methods. **We compared OPN protein levels in human periprosthetic osteolysis tissues with those in osteoarthritis (OA) synovial tissues. To investigate the functions of OPN during particle-induced osteolysis in vivo, titanium particles were implanted onto the calvaria of OPN-deficient mice and their wild-type (WT) littermates. Mice were killed on day 10 and evaluated immunohistologically. The effects of OPN deficiency on the secretion of inflammatory cytokines were examined using cultured bone marrow–derived macrophages (BMMs). BMMs from OPN-deficient and WT mice were cultured with titanium particles for 12 hours, and the concentrations of inflammatory cytokines in the conditioned media were measured by enzyme-linked immunosorbent assay.**

Results. **Expression of OPN protein was enhanced in human periprosthetic osteolysis tissues as compared with OA synovial tissues. In the particle-induced model of osteolysis of the calvaria, bone resorption was significantly suppressed by OPN deficiency via inhibition of osteoclastogenesis, whereas an inflammatory reaction was observed regardless of the genotype. Results of immunostaining indicated that OPN protein was highly expressed in the membrane and bone surface at the area of bone resorption in WT mice. When BMMs were exposed to titanium particles, the concentration of proinflammatory cytokines, such as tumor necrosis factor α, interleukin-1α (IL-1α), IL-1β, and IL-6, as well as chemotactic factors, such as monocyte chemoattractant protein 1 and macrophage inflammatory protein 1α, in the conditioned medium were significantly reduced by OPN deficiency. Whereas phagocytic activity of BMMs was not attenuated by OPN deficiency, phagocytosis-mediated NF-κB activation was impaired in OPN-deficient BMMs. These data indicated that OPN was implicated in the development of particle-induced osteolysis via the orchestration of pro-/antiinflammatory cytokines secreted from macrophages.**

Conclusion. **OPN plays critical roles in wear debris–induced osteolysis, suggesting that OPN is a candidate therapeutic target for periprosthetic osteolysis.**

Total joint arthroplasty has been a significant advance in the treatment of osteoarthritis (OA), rheumatoid arthritis (RA), and other arthritic diseases affecting the major joints of the upper and lower extremities (1). Despite improvements in implant design and surgical techniques, periprosthetic osteolysis causing

Supported by a 21st Century Global Center of Excellence program grant.

[1]Sadanori Shimizu, MD, PhD, Naoki Okuda, MD, PhD, Kenichi Shinomiya, MD, PhD, Takeshi Muneta, MD, PhD, Masaki Noda, MD, PhD: International Research Center for Molecular Science in Tooth and Bone Diseases, and Tokyo Medical and Dental University, Tokyo, Japan; [2]Norihiko Kato, MD, PhD, Atsushi Okawa, MD, PhD, Yoshinori Asou, MD, PhD: Tokyo Medical and Dental University, Tokyo, Japan; [3]Susan R. Rittling, PhD (current address: The Forsyth Institute, Boston, Massachusetts), David T. Denhardt, PhD: Rutgers University, Piscataway, New Jersey; [4]Kunikazu Tsuji, PhD: International Research Center for Molecular Science in Tooth and Bone Diseases, Tokyo, Japan.

Address correspondence and reprint requests to Yoshinori Asou, MD, PhD, Department of Orthopedic Surgery, Tokyo Medical and Dental University, 1-5-45 Yushima, Bunkyo-ku, Tokyo 113-8519, Japan. E-mail: aso.orth@tmd.ac.jp.

Submitted for publication December 14, 2008; accepted in revised form February 4, 2010.

aseptic loosening of artificial joints remains the most serious problem limiting clinical success (2). Reaction to plastic, metal, and acrylic particles results in the formation of granulation tissue containing macrophages and giant cells (3). Periprosthetic osteolysis often occurs as a result of particle phagocytosis by macrophages, which leads to the secretion of inflammatory cytokines, such as interleukin-1 (IL-1) and IL-6, and chemokines, such as monocyte chemoattractant protein 1 (MCP-1) and macrophage inflammatory protein 1α (MIP-1α) (4–8). This process, in turn, leads to the production of the essential osteoclast differentiation factor, RANKL, by stromal cells and activated T cells. RANKL directly stimulates osteoclastogenesis and bone resorption by binding to its receptor (RANK) on osteoclast precursor cells (9–11).

Osteopontin (OPN) is localized to cell–matrix and matrix–matrix interfaces in mineralized tissues, where it is deposited as the result of osteoclast action (12). OPN expression is increased in response to early proinflammatory cytokines and to mechanical strain in bone (13). OPN binds to a subset of integrin receptors; most notably, it is a well-characterized ligand for $\alpha v\beta 3$ integrin, which is expressed at high levels in osteoclasts and endothelial cells (13,14). Therefore, OPN mediates the inflammatory process and subsequent bone resorption by osteoclasts (13). Because OPN expression is induced by many inflammatory cytokines and is produced by macrophages in response to inflammatory stimuli (12), we hypothesized that OPN might be involved in osteolysis (15,16). Indeed, OPN protein and messenger RNA (mRNA) are expressed by macrophages in periprosthetic tissue from patients with aseptically loosened prostheses (17).

To investigate the role of OPN in bone resorptive disorders, such as ovariectomy-induced bone resorption, ectopic bone resorption, and RA, OPN-deficient mice have been examined (14,18,19). Although these pathologic bone resorption conditions are impaired in OPN-deficient mice, the mice have normal skeletal size and patterning (20). In addition, osteoclasts are morphologically normal in OPN-deficient mice (21).

Since OPN is produced by synovial cells, chondrocytes, and osteoblasts, as well as by osteoclasts, this protein has been suggested to play a role in bone diseases caused by abnormal inflammation (19). However, its function in particle-induced osteolysis remains unknown. The purpose of this study was to investigate the functions of OPN in the process of periprosthetic osteolysis.

MATERIALS AND METHODS

Human periprosthetic tissue collection. Tissue samples were collected from the bone–implant interface membranes of 4 patients undergoing revision surgery for aseptic loosening of total hip replacement prosthesis. Control samples were obtained from the joint synovia of 8 patients undergoing primary total hip replacement surgery for OA. There were no clinical or radiologic signs of infection in any tissue sample analyzed.

OPN protein levels in human tissue samples. Protein from human tissue samples was extracted with the use of BioMasher (Investigen) and CelLytic MT (Sigma). Levels of OPN protein in tissue samples were quantified using a human OPN enzyme-linked immunosorbent assay (ELISA) kit according to the manufacturer's protocol (Immuno-Biological Laboratories). All ELISA results were normalized to tissue protein levels, which were quantified using a bicinchoninic acid protein assay kit (Pierce).

Animals. Wild-type (WT) and OPN-deficient mice on the (C57BL/6 $\times$ 129/Sv)F_2 background were produced as previously described (20). Female OPN-deficient mice and WT littermates (1.5–3-month-old) were used in the experiments. All animal experiments were approved by the animal welfare committee at Tokyo Medical and Dental University.

Particles. Pure titanium particles measuring 1–3 μm in diameter were obtained from Alfa Aesar (lot no. L01H16) and were prepared as previously described (22). Briefly, particles of 1–3 μm in diameter were suspended in phosphate buffered saline at a concentration of 1×10^8/ml, washed in 70% ethanol at room temperature, and dried on a clean bench under ultraviolet radiation.

In vivo mouse calvaria resorption model. Eight healthy female OPN-deficient mice and 9 healthy female WT littermates were anesthetized, and their scalps were incised longitudinally to expose the external cranial periosteum. The periosteum was elevated off the external cortex of the calvarium by sharp dissection. Thirty milligrams of commercially prepared titanium particles was placed directly onto the surface of the bone, and the incision was closed. Mice were killed on day 10 thereafter, and each calvarium was excised, fixed, and decalcified in EDTA. After dehydration and paraffin embedding, serial sections measuring 5 μm in thickness were prepared from the 2-mm frontal bone to the intersection of sutures. For each animal, 3 sections of parietal bones obtained at 400-μm intervals were histochemically stained with hematoxylin and eosin and for tartrate-resistant acid phosphatase (TRAP) activity.

Immunohistochemistry. According to the manufacturer's instructions, OPN protein and TNFα were examined by immunohistochemistry with anti-mouse OPN antibody (product no. 18621; Immuno-Biological Laboratories) and anti-mouse TNFα antibody (product no. sc-1348; Santa Cruz Biotechnology), respectively. Briefly, sections were incubated overnight at 4°C with rabbit anti-mouse OPN antibody (1:20 dilution) and goat anti-mouse TNFα antibody (1:50 dilution). The sections then were incubated at room temperature for 30 minutes with biotinylated goat anti-rabbit IgG antibody and biotinylated rabbit anti-goat IgG antibody, respectively. Thereafter, sections were visualized with peroxidase-conjugated avidin and diaminobenzidine using a Vectastain kit (Vector).

Bone histomorphometry. Histomorphometric measurements were performed with a system consisting of a PC and image analysis software (Image Pro Plus 4.1; Media Cybernetics). Since the sagittal suture is irregular in shape in this model, we excluded from the measurement the area within 400 μm lateral to the sagittal suture so that an accurate assessment of bone resorption area could be obtained. The bone resorption area was measured as the eroded surface (ES) along the superior calvarial surface. The osteoclast surface (OcS) and osteoclast number (OcN) were determined in TRAP-stained sections. Osteoclasts were morphologically identified as large multinucleated cells located on the bone perimeter within resorption lacunae.

In vitro activation of bone marrow–derived macrophages (BMMs). Bone marrow stromal cells were obtained from the femoral bone marrow of OPN-deficient and WT mice. Cells were cultured at a density of 1×10^6/well in 24-well plates for 5 days in α-minimum essential medium (α-MEM)/10% fetal calf serum containing 50 ng/ml of macrophage colony-stimulating factor (M-CSF). To confirm the differentiation of stromal cells into macrophages, cultured cells from WT and OPN-deficient mice were diluted with the same solution and analyzed by fluorescence-activated cell sorting (FACS) for CD11b expression.

BMM cytokine secretion assay. BMMs were isolated from WT and OPN-deficient mice (2 mice for each genotype). BMMs of each genotype were divided into 3 groups, cultured for 12 hours with titanium particles, and the concentrations of TNFα and OPN in the media were measured with ELISA kits according to the manufacturer's protocols (Amersham Biosciences, BioSource International, and Immuno-Biological Laboratories, respectively). Multiplex suspension bead array immunoassays were performed using a Luminex 100 analyzer to identify cytokine protein expression in culture supernatants. A Mouse Cytokine 7-Plex kit (BioSource International) was used to specifically evaluate patterns of IL-1α, IL-1β, IL-6, IL-17, MCP-1, MIP-1α, and RANTES expression according to the user's manual.

BMM phagocytic assay. BMMs obtained from the marrow of the long bones of OPN-deficient and WT mice were cultured for 3 days at a density of 1×10^6 cells in 10-cm dishes and then exposed to fluorescence latex beads (Toray) for 1 hour at 37°C. The percentage of phagocytic macrophages was then analyzed by flow cytometry.

Western blot analysis of IκB degradation. Nucleated bone marrow cells were seeded on 35-mm–diameter dishes at a concentration of 5×10^6/dish. Cells were maintained for 3 days in α-MEM supplemented with 10% fetal calf serum, 100 units/ml of penicillin G, 100 μg/ml of streptomycin sulfate, 250 ng/ml of amphotericin B, and 50 ng/ml of M-CSF. On the third day, cells were exposed to titanium particles for various time periods ranging from 0 to 120 minutes. Cells were solubilized with Cell Lysis Buffer (Cell Signaling Technologies) supplemented with 1 m*M* phenylmethylsulfonyl fluoride and a protease inhibitor cocktail (Complete Mini; Roche Applied Science). Cell lysates (10 μg) were separated in sodium dodecyl sulfate–Tris glycine–polyacrylamide gels (4–20% gradient gel; Invitrogen) and blotted on to polyvinylidene difluoride membranes (Bio-Rad). The membranes were stained with anti-mouse IκBα polyclonal antibody (BioVision Research Products), and signals were visualized with a Vectastain Elite ABC kit (Vector). Membranes were reblotted with anti-mouse β-actin antibody (Santa Cruz Biotechnology) as a sample loading control.

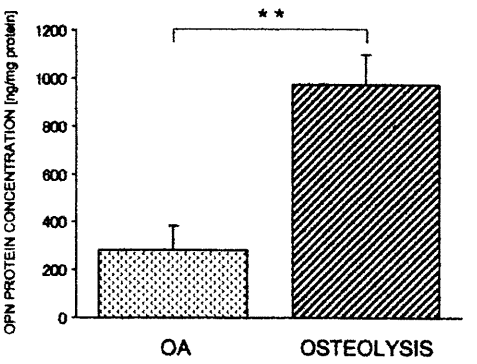

Figure 1. Osteopontin (OPN) protein levels in human periprosthetic osteolysis tissues. OPN protein levels were increased in interface membranes and capsules from aseptically loosened total hip implants (osteolysis) as compared with osteoarthritis (OA) synovium. Values are the mean and SEM. ** = $P < 0.001$.

Statistical analysis. Data are expressed as the mean ± SEM. Statistical evaluation was performed with the Mann-Whitney U test. *P* values less than 0.05 were considered significant.

RESULTS

Enhanced expression of OPN protein in human periprosthetic osteolysis tissues. We compared OPN protein expression levels in the interface membranes and capsules from patients with aseptically loosened total hip implants with the OPN protein expression in OA synovium (Figure 1). The findings of ELISA indicated that OPN protein was strongly increased in the periprosthetic osteolysis tissues.

Protection of OPN-deficient mice from particle-induced osteolysis. To investigate the function of OPN in particle-induced osteolysis, we used a previously established in vivo mouse calvaria resorption model that closely resembles aseptic loosening in humans (22). The calvariae of WT mice exposed to titanium particles generated a supracranial inflammatory response consisting of a fibrous membrane associated with abundant mononuclear cells (Figure 2A), which were identified by their morphometric appearance as being macrophages, foreign-body giant cells, fibroblasts, and osteoclasts. Importantly, these membranes contained numerous juxtacortical osteoclasts (Figures 2A, C, and E). Whereas the calvariae of OPN-deficient mice exposed to titanium particles generated an inflammatory membrane similar to that seen in WT animals (Figure 2B), the titanium

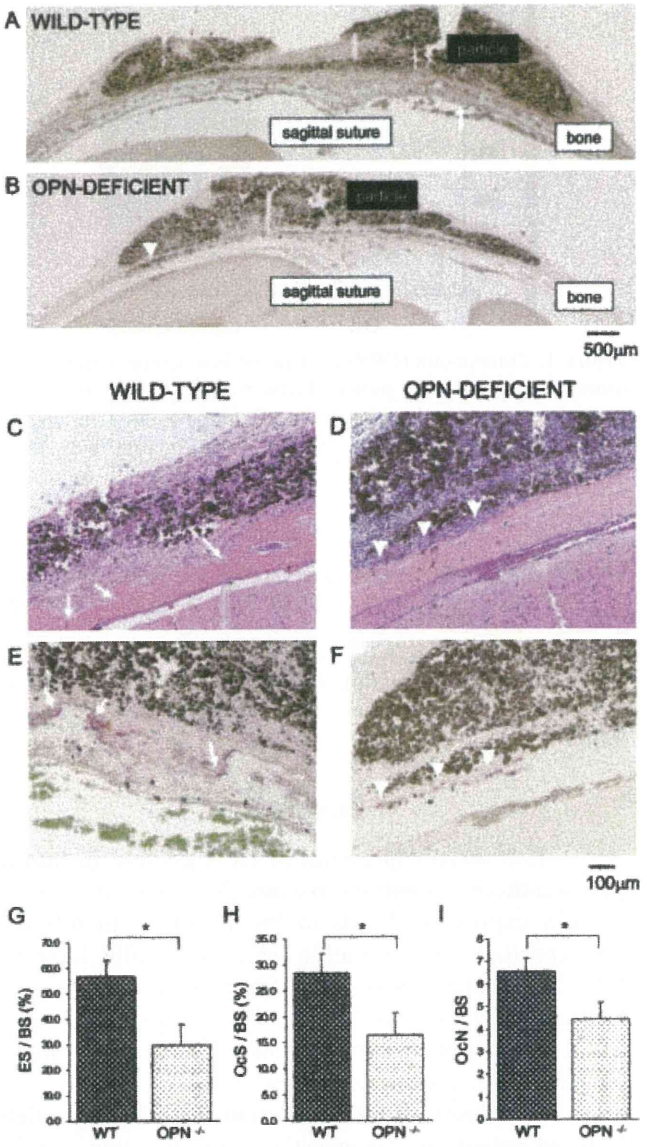

Figure 2. Protection of osteopontin (OPN)–deficient mice from particle-induced osteolysis in an in vivo calvaria resorption model. Sections of calvaria from wild-type (WT) or OPN$^{-/-}$ mice were stained with hematoxylin and eosin (**C** and **D**) and for tartrate-resistant acid phosphatase activity (**A**, **B**, **E**, and **F**). **A** and **B,** Sections of whole calvaria from a WT mouse and an OPN$^{-/-}$ mouse. **C–F,** Higher-magnification views of calvarial sections from WT and OPN$^{-/-}$ mice. Inflammatory reactions consisting of a fibrous membrane and osteoclastic bone resorption were widespread in WT mice (**arrows** in **A, C,** and **E**). These reactions were less severe in OPN$^{-/-}$ mice (**arrowheads** in **B, D,** and **F**). **G–I,** Quantification of particle-induced osteolysis and osteoclastogenesis. The eroded surface/bone surface (ES/BS) (**G**) measure indicates the bone resorption area on the superior calvarial surface >400 μm away from the sagittal suture. The osteoclast surface/bone surface (OcS/BS) (**H**) and osteoclast number/bone surface (OcN/BS) (**I**) measures were also determined outside of the suture area. Values are the mean and SEM. * = $P < 0.05$.

particle–induced bone resorption was attenuated in these animals (Figures 2B, D, and F). No enhancement of bone resorption activity was observed regardless of the genotypes in sham-operated mice (results not shown).

TRAP staining revealed the presence of osteoclasts in each resorption pit (Figures 2A, B, E, and F). However, the bone resorption area (representing the ES/bone surface [BS]) on the cortex was significantly reduced in osteolysis-induced OPN-deficient mice as compared with their WT littermates (Figure 2G). The OcS/BS and the OcN/BS were also significantly reduced in OPN-deficient mice as compared with their WT littermates (Figures 2H and I). Thus, osteoclastogenesis was impaired by OPN deficiency in this model.

Bone resorption lacunae were observed even in OPN-deficient osteoclasts. However, each bone resorption pit on the surface of OPN-deficient calvaria was shallow (Figures 2F and 3B), whereas penetration of the calvaria cortex was observed in WT animals as a result of active bone resorption (Figures 2E and 3A). The depth and area of each bone resorption pit were significantly reduced by OPN deficiency (Figures 3C and D). These data indicated that the function of each osteoclast was attenuated by OPN deficiency.

Enhanced expression of OPN protein and TNFα in mice with particle-induced osteolysis. Immunohistologic examination revealed that OPN protein was highly

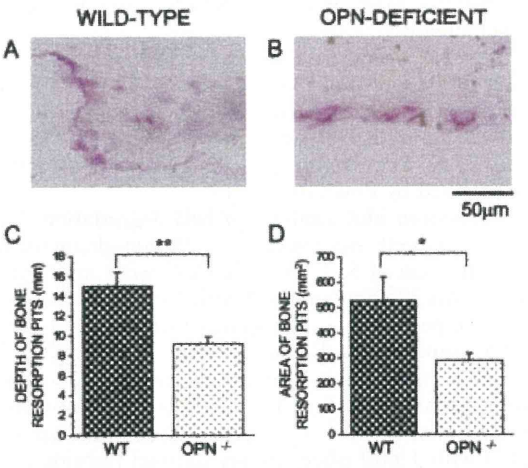

Figure 3. Smaller bone resorption pits in osteoclasts from osteopontin (OPN)–deficient mice. **A** and **B,** Morphologic features of osteoclasts from wild-type (WT) and OPN$^{-/-}$ mice. **C** and **D,** Quantification of the depth (**C**) and area (**D**) of bone resorption pits. Bone resorption pits were measured in high-power micrographs of tartrate-resistant acid phosphatase–stained sections. Values are the mean and SEM. ** = $P < 0.001$; * = $P < 0.05$.